Gut Microbiota Alterations and Cognitive Impairment Are Sexually Dissociated in a Transgenic Mice Model of Alzheimer's Disease

Daniel Cuervo-Zanatta[a,b], Jaime Garcia-Mena[b,*] and Claudia Perez-Cruz[a,*]

[a]*Pharmacology Department, Center for Research and Advanced Studies of the National Polytechnic Institute (Cinvestav), Laboratory of Neuroplasticity and Neurodegeneration, Mexico City, Mexico*
[b]*Genetics and Molecular Biology Department, Center for Research and Advanced Studies of the National Polytechnic Institute (Cinvestav), Laboratory of reference and support for the characterization of genomes, transcriptomes and microbiomes, Mexico City, Mexico*

Abstract.

Background: Normal aging is accompanied by cognitive deficiencies, affecting women and men equally. Aging is the main risk factor for Alzheimer's disease (AD), with women having a higher risk. The higher prevalence of AD in women is associated with the abrupt hormonal decline seen after menopause. However, other factors may be involved in this sex-related cognitive decline. Alterations in gut microbiota (GM) and its bioproducts have been reported in AD subjects and transgenic (Tg) mice, having a direct impact on brain amyloid-β pathology in male (M), but not in female (F) mice.

Objective: The aim of this work was to determine GM composition and cognitive dysfunction in M and F wildtype (WT) and Tg mice, in a sex/genotype segregation design.

Methods: Anxiety, short term working-memory, spatial learning, and long-term spatial memory were evaluated in 6-month-old WT and Tg male mice. Fecal short chain fatty acids were determined by chromatography, and DNA sequencing and bioinformatic analyses were used to determine GM differences.

Results: We observed sex-dependent differences in cognitive skills in WT mice, favoring F mice. However, the cognitive advantage of females was lost in Tg mice. GM composition showed few sex-related differences in WT mice. Contrary, Tg-M mice presented a more severe dysbiosis than Tg-F mice. A decreased abundance of *Ruminococcaceae* was associated with cognitive deficits in Tg-F mice, while butyrate levels were positively associated with better working- and object recognition-memory in WT-F mice.

Conclusion: This report describes a sex-dependent association between GM alterations and cognitive impairment in a mice model of AD.

Keywords: Anxiety, APP/PS1 mice, dysbiosis, high-throughput DNA sequencing, short-chain fatty acids, spatial memory, wildtype littermates

*Correspondence to: Claudia Perez-Cruz, Pharmacology Department, Center for Research and Advanced Studies of the National Polytechnic Institute (Cinvestav), Laboratory of Neuroplasticity and Neurodegeneration, Av Instituto Politécnico Nacional 2508, San Pedro Zacatenco, Gustavo A. Madero, 07360 Mexico City, CDMX, Mexico. E-mail: cperezc@cinvestav.mx. and Jaime Garcia-Mena, Genetics and Molecular Biology

Department, Center for Research and Advanced Studies of the National Polytechnic Institute (Cinvestav), Laboratory of reference and support for the characterization of genomes, transcriptomes and microbiomes, Av Instituto Politécnico Nacional 2508, San Pedro Zacatenco, Gustavo A. Madero, 07360 Mexico City, CDMX, Mexico. E-mail: jgmena@cinvestav.mx.

INTRODUCTION

Alzheimer's disease (AD) is the most common cause of dementia, affecting around 50 million people worldwide [1]. This debilitating disorder is marked by the aggregation of two proteins: amyloid-β, which accumulates in plaques, and tau, which can become hyperphosphorylated and aggregates in neurofibrillary tangles [1]. Despite the recent advance in the understanding of AD pathology, the exact etiology continues to be debated, impeding further development of effective therapies to treat or prevent this neurodegenerative disease.

Several risk factors have been associated with AD, such as lack of primary education, metabolic alterations, smoking, depression, and *APOE ε*4 genotype, among others [2]. Women had an 1.6-fold increase in AD incidence than men [3, 4], and this higher prevalence has been linked to the abrupt decline in sex hormones after menopause, and length of estrogen exposure during life [5, 6].

Cognitive abilities showed a sex dimorphism in young and old healthy subjects [7] as women showed advantages in object location memory [8, 9] and visual memory for objects [10, 11] over men. Contrary to this observation, male cognitive advantage is found on tests of mental rotation of spatial stimuli [12, 13] compared to females. With aging, however, this cognitive dimorphism in healthy subjects seems to be reversed or lost [14–16], with a worst [17–20] or better cognitive performance in men than women [14], or equal cognitive decline between genders [21].

Those conflicting results can be harmonized if we take in account the task and the related memory that was assessed. In early stages of AD, women showed still a better cognitive performance than age-matched men, but at advance stages of the disease, this cognitive advantage is lost [15, 22–26]. The Alzheimer's Disease Neuroimaging Initiative (ADNI) study shows that during amnestic mild cognitive impairment (MCI), females performed better in verbal memory compared to males. However, high levels of amyloid burden associates with a loss of this female cognitive advantage [22–24], as no sex-related differences were observed on block design [27] and visuoconstructive tests [28] in AD patients. Notwithstanding, AD pathological hallmarks showed a sexual dimorphism that is present even in late stages of the disease, as AD women present more neuritic plaques and neurofibrillary tangles compared to aged-matched men [29]. In contrast, another study claimed that no difference in the prevalence of senile plaques

or neurofibrillary tangles was found by gender [30]. The use of animal models may help to better elucidate the sex-related differences in AD pathology, as human data shows conflicting results. Age-matched female and male transgenic (Tg) mice have an identical genetic background; therefore, the pathological and cognitive differences may be associated only with sex. At 15–19 months of age, female Tg2576 mice present more amyloid plaques than their male counterparts [31]. Similarly, a stronger plaque burden was observed in female APP/PS1 Tg mice compared to males [32, 33]. Despite the greater amyloid burden developed in aged female Tg mice, no worst cognitive decline is observed compared to males [34]. Emerging research proposes that the gut microbiota (GM) could play a central role in the regulation of emotions and cognition [35, 36]. Alterations in the GM seems to accompany aging [37, 38], where a decreased bacteria diversity and a pro-inflammatory profile dominates GM in aged people [39, 40]. Moreover, recent evidence suggests that GM could play a major role in AD, as lower GM diversity is observed in AD patients compared to aged-matched healthy subjects [41–46]. So far, these studies have not discriminated the sex factor in their results, despite women's higher incidence of AD. Experiments carried out in AD mice models showed a reduction in amyloid pathology after antibiotic-treatment in APP/PS1 male mice, but not in female mice [47]. Females' GM antibiotic resistant effect deserves attention, as it may underlie important etiological factors associated with females' vulnerability to develop AD. Therefore, it is necessary to determine the differences in the GM presented in female and male Tg mice, as well as describe the possible interaction between microbial communities and cognition as possible factor associated with women's greater vulnerability to develop AD.

MATERIALS AND METHODS

Experimental design

Hemizygous APP/PS1 male (Tg-M) and female (Tg-F) mice expressing a chimeric mouse/human amyloid precursor protein (Mo/HuAPP695swe) and a mutant human presenilin 1 (PS1-dE9) transgene on a C57BL/6 genetic background (Jackson Laboratory, Bar Harbor, ME, USA, RRID: MMRRC-34829-JAX) and their wild-type (WT) littermates (males, WT-M and females, WT-F) were used for the study. Animal management was supervised by licensed veterinarian care and approved by the Bioethics

Committee of the Center for Research and Advanced Studies of the National Polytechnic Institute (Cinvestav) in accordance with the Mexican official standard NOM-062-ZOO-1999 and the principles set forth in the 8th edition of the National Institute of Health (NIH) guide for the care and use of laboratory animals and endorsed by the Institute for Laboratory Animal Research, the Division on Earth and Life Studies, and the National Research Council of the National Academies. Once animals reached 4 months of age, they were individually housed with *ad libitum* access to food (AIN-93 diet) [48] and water under optimal vivarium conditions (12 h/12 h light–dark cycle, 20°C, and 40–50% relative humidity) for 2 months.

Estrous cycle evaluation

Cognitive evaluations in female mice were done only during the metaestrous/diestrous, the reproductive stages with the lowest hormonal levels [49], as estradiol have a direct impact in cognition and memory [50]. Cytology and typification of the reproductive stage was based on previous descriptions [51, 52].

Cognitive assessment

One week before sacrifice, behavioral testing was performed. To habituate the animals for the behavioral tests, animals were placed in the behavioral room 2 days before start testing trials. Anxiety-related behaviors were assessed by the Elevated Plus Maze (EPM) [50]. Briefly, the 50 cm elevated plus-shaped maze was made of medium-density fiberboard with a matte black acrylic surface and four arms (50 cm long and 10 cm wide) where two arms were open, and two arms were enclosed by 30 cm height walls. The task consisted of one trial per animal, where the animals were placed in the center of the EPM facing an open arm. Usually, rodents avoid open spaces and spend most of the time in enclosed places, such as the closed arms of the EPM [50]. Entries into the open/close arms were recorded during 5 min, and the animal's trajectory was used to calculate percentage of time spent in each arm [50] (Fig. 1A, B).

Working memory was evaluated by the T-maze (TM) [53]. The TM is an appropriate test to evaluate hippocampal and PFC functions in rodents [54] and to examine cognitive deficits in early stages of AD pathology [55]. Briefly, a T-shaped maze apparatus of polymethylmethacrylate with starting

arm ($8.5 \times 10.5 \times 33.0$ cm), and two choice arms ($8.5 \times 10.5 \times 30.0$ cm each, left and right) was used as previously described [56]. The TM task consisted of two phases: 1) Sample phase, animals were placed at the start arm and allowed to choose between left or right choice arms. A central divider was then inserted into the start arm to create a start box. Once animals have chosen an arm, they were confined there for 30 s, thereafter the door was reopened and allow mice to return to the start arm, where animals were removed and returned to their cage. 2) Choice phase, 2 min later, animals were placed again in the start arm without the central divider and allowed them to choose an arm. When animals faced the TM apparatus, they display a tendency to alternate and avoid the entry into the previously entered arm. If the animal chooses two different arms in both phases, this is counted as spontaneous alteration. Two hours later the procedure was repeated. Three trials were given on each day for 2 days, with a total of 6 trials per animal. Percentage of spontaneous alternations were calculated from total of correct arm entries (Fig. 1C).

Recognition memory was evaluated by the Novel Object Recognition task (NOR) [57]. NOR is an appropriate test to evaluate recognition memory related to hippocampus [58] and prefrontal cortex (PFC) [59] functions, both regions heavily affected in AD [56]. This task is based on the natural tendency of rodents to explore a novel object more than a familiar one [57]. NOR test was carried out in a 40 cm^2 open field arena with 40 cm height walls of plywood surrounding the floor. NOR task consisted of three phases: 1) Habituation phase: animals explored the open field for 5 min without objects in the box; 2) Training phase: Twenty-four hours after habituation phase, animals were placed for 5 min in the box from the same starting position, and with two objects with identical features (weight, size, texture, shape and color) positioned in adjacent corners at 10 cm from the walls; 3) Trial phase: The recognition memory test was carried out 1.5 h after the training trial with the mice exploring the open field for 5 min in the presence of one familiar and one novel object, this last one different features than the former. A discrimination index (DI) was calculated for each animal after the test session (Fig. 1D) as DI = (time with novel object — time with familiar object) / (time with novel object+time with familiar object). Between all testing trials, all surfaces and objects were washed with 40 % ethanol solution. Exploration was defined as smelling and/or touching the object with the nose and/or forepaws [57].
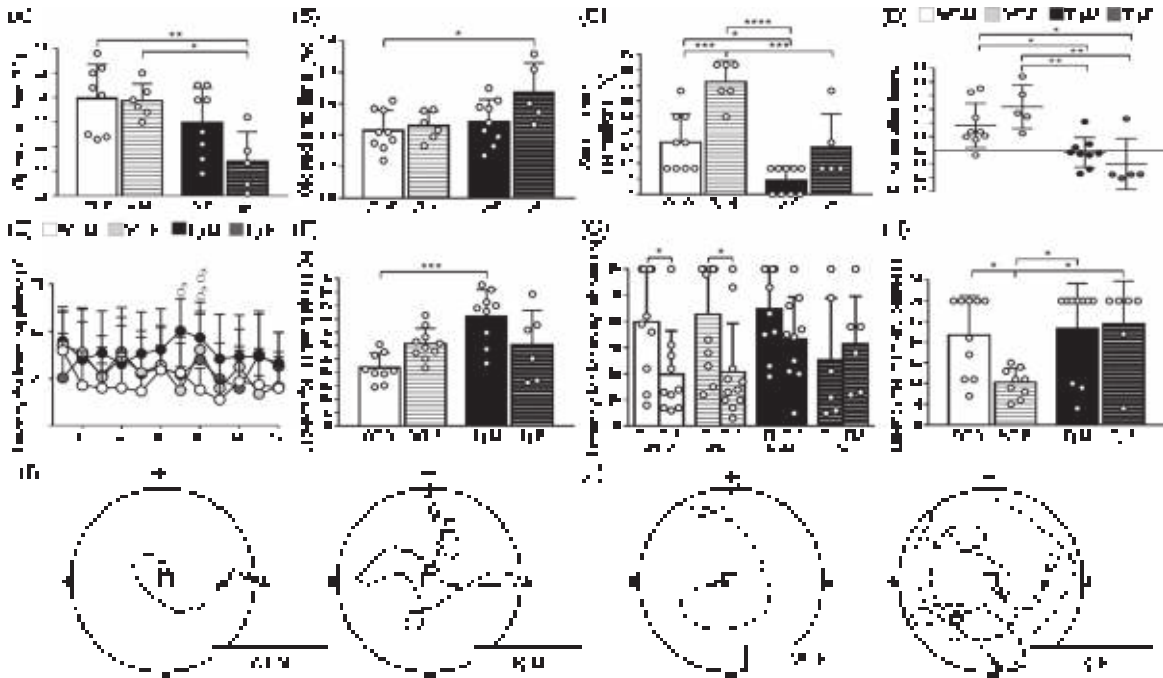
Fig. 1. Effect of gender and genotype in anxiety and memory performance. A) Anxiety was inversely proportional to the time spent in the open arm [F (1, 23) = 2.35, 3.03 and 12.42 for interaction, row and column factor respectively] and B) directly proportional to the time spent in the closed arms [F (1, 25) = 2.15, 4.07 and 6.30 for interaction, row and column factor respectively] in the elevated plus maze. C) Working memory was directly proportional to the spontaneous alternations [F (1, 25) = 2.25, 24.31 and 30.05 for interaction, row and column factor respectively] in the T-maze. D) Recognition memory was directly proportional to the discrimination index [F (1, 24) = 3.50, 0.18 and 26.80 for interaction, row and column factor respectively] in the novel object recognition test. E) Spatial learning curves show the latency to find the hidden platform during learning phase [F (33, 396) = 1.03, F (11, 396) = 1.69 and F (3, 396) = 14.68 for interaction, row and column factor respectively] in the WM. X axis corresponds to the 12 consecutive learning assays. F) Spatial learning was inversely proportional to the latency to find the platform during learning phase [F (1, 30) = 10.95, 0.09 and 10.07 for interaction, row and column factor respectively] in the water maze. G) Learning performance was compared between trial 1 and 12 during learning phase in the WM. H) Spatial memory was inversely proportional to the latency to find the place where the platform was originally located [F (1, 31) = 4.02, 2.80 and 6.34 for interaction, row and column factor respectively] during WM memory phase. I) Representative schemes of WT-M and Tg-M mice trajectory for spatial learning trials from the start point to the platform area. J) Representative schemes of WT-F and Tg-F mice trajectory for the spatial memory trial from the start point to the platform area. Cardinal points are marked in maze walls as a star-shaped polygon (north), a square (south), a triangle (west), and a circle (east). Black arrow indicates start point, white arrow indicates finish point, central square indicates platform area and dotted line indicates mouse trajectory in the WM test. For A, WT-M *n* = 9, WT-F *n* = 7, Tg-M *n* = 9, and Tg-F *n* = 6. For B and C, WT-M *n* = 10, WT-F *n* = 7, Tg-M *n* = 10, and Tg-F *n* = 6. For D, WT-M *n* = 10, WT-F *n* = 6, Tg-M *n* = 10, and Tg-F *n* = 6. For E, F, and G, WT-M *n* = 10, WT-F *n* = 11, Tg-M *n* = 10, and Tg-F *n* = 6. For H, WT-M *n* = 10, WT-F *n* = 9, Tg-M *n* = 10, and Tg-F *n* = 6. For A-C and F-H, white color circles within bars indicate experimental subjects. For D and E, white, grey and black circles indicate experimental groups. Data are shown as mean ± SD bars. For A-F and H, two-way ANOVA with Tukey *post-hoc* correction was performed comparing experimental groups. For G, unpaired *t* tests were performed comparing learning assay no.1 with no. 12 for each experimental group. For A-F and H, data between square brackets indicate F (DFn, DFd) values of two-way ANOVA with Tukey *post-hoc* corrections. Statistical significances are shown as *p < 0.05, **p < 0.01, ***p < 0.001, and ****p < 0.0001. For E, statistical significance between WT-M versus WT-F is shown by □, Tg-M versus Tg-F by ○, WT-M versus Tg-F by △, WT-F versus Tg-M by #, WT-M versus Tg-M by ♂ and WT-F versus Tg-F by ♀ one symbol represents *p < 0.05, two symbols *p < 0.01, three symbols *p < 0.001, and four symbols *p < 0.0001. T1 = learning trial no. 1, T12 = learning trial no.12, F, female; M, male; Tg, transgenic; WT, wild type.

Spatial memory was assessed by Water Maze (WM) [60]. The WM is an appropriate test to evaluate spatial memory related to hippocampus [61] and PFC [62] functions. Briefly, the WM task was carried out in a 100 cm diameter and 30 cm height round pool half filled with 26°C white water and an escape platform located in the center, as previously described [60]. Spatial clues were posted on each wall of the room with paper figures of different shapes and colors. WM task consisted of three phases, followed by an adaptation phase that consisted of placing the mice for 20 s on the scape platform visible for the animal: 1) Training phase: mice were released and allowed to swim in order to reach the scape platform in a maximum time of 60 s. This phase was repeated three times, each starting from a different cardinal point.

2) Learning phase: the animal was allowed to swim in order to find the hidden scape platform in a maximum time of 60 s for 12 consecutive trials, starting 3 non-consecutive times from different cardinal points. 3) Memory phase: immediately after all animals have completed the 12 consecutive learning trials, they performed 1 probe trial, in which the scape platform was removed from the pool. The animal was released from the north and allowed to swim to find the missing platform in a maximum time of 30 s. The time spent (latency) to find the hidden platform (learning phase) and the platform area (memory phase) in the pool was recorded and assigned as an inversely proportional measure to the spatial learning and memory respectively (Fig. 1E-H). Experiments were recorded with a Logitech DH Pro Webcam C920 camera connected to a computer equipped with Logitech Capture 1.10.110 with the Eniima software (inhouse made software) in order to track animal's behavior and trajectory (Fig. 1I, J).

Determination of short chain fatty acids in feces

Fecal samples were collected for each animal before the cognitive tests. Animals were placed for 1 h in a Super Mouse 750™ Micro-Isolator® system cage for housing mice (15 cm width x 30 cm long x 17 cm high) previously cleaned and disinfected. At least 100 mg of feces pellets were collected per animal, immediately frozen and store at –70°C until use, for short-chain fatty acids (SCFAs) determination or microbiota analysis.

For SCFAs determination, the collected fecal samples were dried to constant weight and subsequently processed using the solid-phase extraction (SPE) method to analyze via HPLC (PerkinElmer Series N3896). At least 50 mg of dried feces were suspended completely in 1 ml of deionized water by vigorous mixing in a vortex at maximum speed for 10 min. The suspension was centrifuged at 13000 rpm for 10 min, the supernatant was transferred to a fresh tube and passed through activated C-18 max 100 mg/mL GracePure™ Reversed-Phase SPE Columns according to the manufacturer's instructions as previously described [63]. The SCFAs were eluted with 1 mL of filtered water (Nylon Syr Filter, 13 mm, 0.22 μm) and analyzed via HPLC using 20:80 acetonitrile:NaH_2PO_4 (J.T. Baker No. 9012-03 and Sigma-Aldrich No. S8282 respectively) at a pH of 2.2 using phosphoric acid, (J.T. Baker No. 0260-05) as mobile phase [64]. Standard curves were prepared for acetate (Sigma-Aldrich No. 45754-100ML-F),

propionate (Sigma-Aldrich No. P1386-500ML), and butyrate (Sigma-Aldrich No. B103500-500ML). SCFAs proportion was calculated taking the total amount of acetate + propionate + butyrate for each experimental subject as 100%.

Fecal microbiota analysis

Bacterial DNA was extracted using the Favor-Prep™ Stool DNA Isolation Mini Kit (Favorgen Biotech Corp, Cat. No: FASTI001-1) according to the manufacturer´s instructions. The purified DNA quantity was measured using 260/280 nm absorbance using a Nano Drop 2000 spectrophotometer (Thermo Scientific), and its quality was evaluated by 0.5% agarose gels electrophoresis. Genomic libraries of ∼281 base pairs (bp) 16S rDNA 3rd hypervariable region (V3) amplicons were generated for each experimental subject using specific V3-341F primers against V3 that also contained a different 12-bp Golay barcode (set of barcodes 1–100) complementary to position 340–356 of *Escherichia coli* 16S rRNA molecule *rrnB* GeneBank J01859.1 and an overhang adapter specified by Ion Torrent, and V3-518R reverse primers complementary to position 517–533 of the same molecule [65]. The amplicons of the V3 regions were generated by 1X 50 μl polymerase chain reactions (PCR) containing 1 μl of 10 μM forward primer, 1 μl of 10 μM reverse primer (settings specified above), 0.25 μl of 5 U/μl high thermostable DNA recombinant polymerase (Thermo Scientific No. EP0402), 1 μl of 10 mM dNTP mix (Thermo Scientific No. R0191), 4 μl of 25 mM $MgCl_2$ (Thermo Scientific No. R0971), 5 μl of 10X taq buffer with KCl (100 mM Tris-HCl [pH = 8.8 at 25°C], 500 mM KCl and 0.8% volume/volume [% v/v] nonidet P40, Thermo Scientific No. B38) and 20 ng of genomic DNA in 37.75 μl of nuclease-free water (Thermo Scientific No. R0581) per reaction. Amplification was carried out using Applied Biosystem Veriti Thermal Cycler (Supplementary Table 1). For sequencing, equivalent amounts of 1 to 100 barcoded amplicons (∼10 μg each) were combined. Each mix was purified using E-Gel iBase Power System (Invitrogen). The libraries size and concentration were determined using an Agilent 2100 Bioanalyzer, and libraries for each run were adjusted to 26 pM prior to clonal amplification. Emulsion PCR was carried out using the Ion OneTouch™ 200 Template Kit v2 DL (Life Technologies), according to the manufacturer´s instructions. Amplicon enrichment with ion spheres was done using Ion
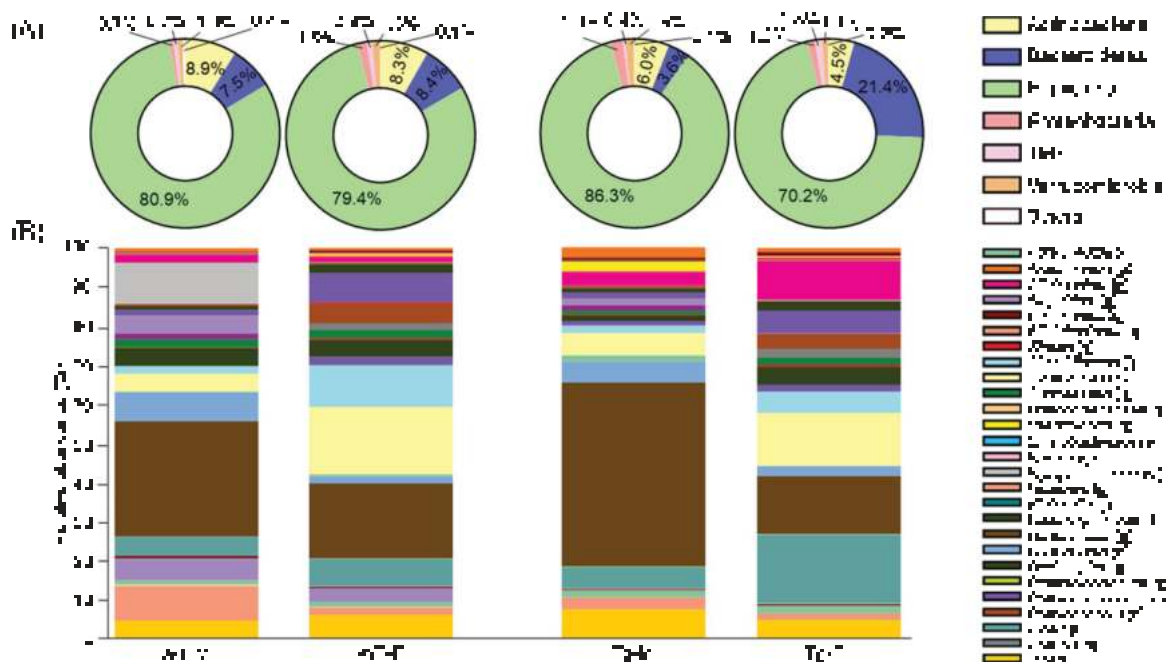
Fig. 2. Relative abundance of bacterial *taxa* in fecal samples. A) Pie charts of *phyla*'s relative abundance. The numbers on/beside charts indicate the percentage of abundance. For A, the color of each tag indicates bacterial *phyla*. Others refers to *phyla* abundances <0.1% of relative abundance. B) Relative abundance of bacterial *taxa*. The color of each tag indicates order, family and genus bacterial *taxa*. Others refers to *taxa* <0.5% of relative abundance. WT-M *n* = 9, WT-F *n* = 8, Tg-M *n* = 6, and Tg-F *n* = 6. Data are shown as mean. Complete abundances and statistical significances are shown in Table 1. F, female; f, family; g, genus; M, male; o, order; Tg, transgenic; WT, wild type.

OneTouch ES. The sequencing was done using the Ion 316 Chip Kit v2 and the Ion Torrent Personal Genome Machine (PGM) System. After sequencing, reads were filtered by the PGM software to remove low quality and polyclonal sequences. During this process, sequences matching the 3′ adapters were automatically trimmed and filtered. Ion Torrent PGM software, Torrent Suite v4.0.2, was used to demultiplex the sequenced data based on their barcodes. Poor quality reads were eliminated from the datasets, i.e., quality score ≤20, containing homopolymers >6, length <200 nucleotides (nt), and containing errors in primers or barcodes. Filtered data were exported as FASTQ files. Demultiplexed sequencing data were analyzed using quantitative insights into microbial ecology (QIIME) software v1.9.0 pipeline [66]. FASTQ files were converted into FASTA files, and all demultiplexed files were concatenated into a single file. Closed reference operational taxonomic units (OTUs) were determined at the 97% similarity level using the UCLUST algorithm. Chimeras were detected and removed from the datasets using the ChimeraSlayer. Sequence alignments were done against the Greengenes 13.9 core set (sequencing

summary is shown in Supplementary Table 2). Microbial sequence data were pooled for OTUs analysis and comparison of taxonomic relative abundance was obtained (Figs. 2 and 3, Supplementary Figure 1, Table 1, and Supplementary Table 3). Prior to calculate microbial diversity, the OTU table was rarefied at 8,700 sequences per sample (samples with <8,700 were omitted) using a "single_rarefaction.py" QIIME script for alpha diversity metrics. *Taxa* richness measurements (Observed and Chao1) and alpha diversity indexes (Shannon and Simpson) were calculated (Fig. 4A, Table 2, and Supplementary Figure 2). Weighted and unweighted UniFrac distances were used to perform the principal coordinate analysis (PCoA; Fig. 4B). Community diversity was determined by the number of OTUs and beta diversity, measured by UniFrac unweighted and weighted distance matrices in QIIME software v1.9.0. Analysis of similarities (ANOSIM) and permutational multivariate analysis of variance (ADONIS), were used to determine statistically significant clustering of groups based upon microbiota structure distances. Furthermore, linear discriminant analysis (LDA) effect size (LefSe) program v1.0 was used to per-
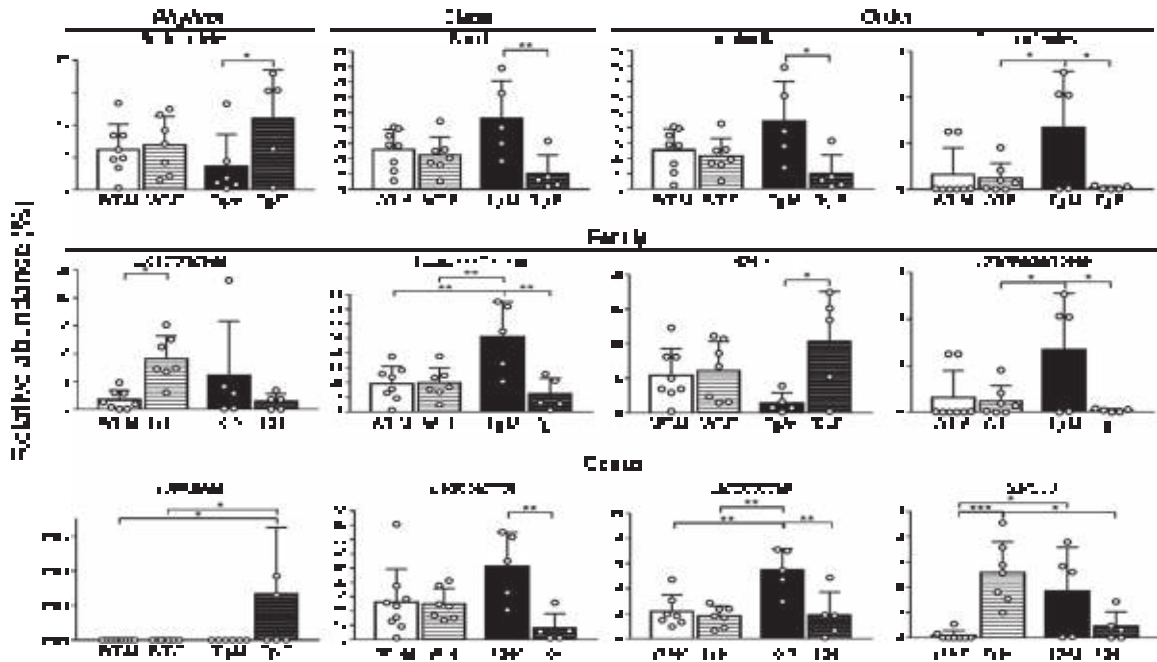
Fig. 3. Relative abundance of prominent bacterial *taxa* in fecal samples. Relative abundance values of Bacteroidetes [F (1, 21) = 5.20, 6.93 and 0.92 for interaction, row and column factor respectively], Bacilli [F (1, 21) = 6.38, 9.92 and 0.42 for interaction, row and column factor respectively], Lactobacillales [F (1, 21) = 5.24, 8.15 and 0.29 for interaction, row and column factor respectively], Turicibacterales [F (1, 21) = 5.27, 6.69 and 2.29 for interaction, row and column factor respectively], *Clostridiaceae* [F (1, 21) = 8.99, 0.44 and 0.64 for interaction, row and column factor respectively], *Lactobacillaceae* [F (1, 21) = 11.16, 10.98 and 4.26 for interaction, row and column factor respectively], *S24-7* [F (1, 21) = 4.96, 6.54 and 0.003 for interaction, row and column factor respectively], *Turicibacteraceae* [F (1, 21) = 5.20, 6.60 and 2.34 for interaction, row and column factor respectively], *Klebsiella* [F (1, 25) = 0.05 for interaction, row and column factor], *Lactobacillus* [F (1, 22) = 7.59, 8.67 and 0.30 for interaction, row and column factor respectively], *Lactococcus* [F (1, 21) = 7.50, 11.60 and 8.23 for interaction, row and column factor respectively] and *SMB53* [F (1, 21) = 20.96, 1.55 and 0.17 for interaction, row and column factor respectively] present in fecal samples are shown. WT-M $n = 9$, WT-F $n = 8$, Tg-M $n = 6$, and Tg-F $n = 6$. White color circles within bars indicate experimental subjects. Data are shown as mean. Data between square brackets indicate F (DFn, DFd) values of two-way ANOVA with Tukey *post-hoc* correction. Statistical significances are shown as $*p < 0.05$, $**p < 0.01$, $***p < 0.001$, and $****p < 0.0001$. Complete abundances and statistical significances are shown in Table 1 and Supplementary Table 3. F, female; M, male; Tg, transgenic; WT, wild type.

form LDA (scores ≥2; Fig. 5 and Supplementary Table 4) in order to estimate significant effect size of each bacterial *taxa* between experimental groups [67].

Metagenome prediction

We used Phylogenetics Investigation of Communities by Reconstruction of Unobserved States (PICRUSt v.1.1.1) in order to predict related metabolic profiles of the metagenomes from 16S rDNA gene data set by Kyoto Encyclopedia of Genes and Genomes (KEGG) orthologs classification database at hierarchy level 3 pathways. Statistical Analysis of Taxonomic and Function (STAMP v2.1.3) software was used to determinate significant differences in abundance of OTUs related to metabolic pathways (Fig. 6 and Supplementary Table 5) [68].

Correlations between determined parameters

Associations between cognition, SCFAs concentration and proportion, bacterial *taxa* relative abundance, microbial diversity, and proportion of predicted metabolic pathways-related sequences were assessed by Pearson's correlation coefficient (GraphPad Prism version 6) (Fig. 7).

Statistical analysis

Data are expressed as the mean ± standard deviation (SD). Open arm time, closed arms entries, spontaneous alternations, DI, WM latencies, SCFAs concentration and proportion, GM relative abundances, alpha diversity indexes, food intake, and body weight changes were analyzed by a two-way ANOVA followed by a Tukey *post-hoc* test. Beta diversity was analyzed by ANOSIM and ADONIS,

Table 1
Fecal microbiota relative abundance (%) reported in Figures 2 and 3

Taxa	WT-M	WT-F	Tg-M	Tg-F
Firmicutes (p)	75.7119	81.8732	81.293	73.4341
Actinobacteria (p)	16.7785	7.4523	5.383	3.9604
Bacteroidetes (p)	5.7831	8.0194	6.4088	19.0961°
Verrucomicrobia (p)	1.1459	0.718	2.9396	1.048
Proteobacteria (p)	0.3247	1.2157	3.3628	1.2433
TM7 (p)	0.2041	0.6366	0.5097	1.0352
Others (p)	0.0513	0.0848	0.1027	0.1829
Clostridiales (o)	4.9036	18.3429	6.3821	14.2808
Erycipelotrichaceae (f)	11.022	0.11803	0.0232	0.18556
S24-7 (f)	5.0183	0.07403	5.8484	0.18384°
Lachnospiraceae (f)	4.8664	4.58625□	1.5317	4.88957
Clostridiaceae (f)	1.6447	11.1083□	1.7642	5.49927
Ruminococcaceae (f)	1.4862	7.66618	1.5629#	5.94374
Coriobacteriaceae (f)	0.4584	0.2753	0.0141	0.023
Enterobacteriaceae (f)	0.0247	0.0077	0.0293	0.0053
Lactobacillus (g)	30.9196	20.3754	50.7033♂♂	15.5784°°
Bifidobacterium (g)	9.2151	2.0181	3.2659	1.7438
Lactococcus (g)	7.7709	1.8941	5.8340♂♂##	2.6664°°
Atopobium (g)	5.9431	3.7677	0.0155	0.0022
Ruminococcus (g)	4.6284	0.0108	1.7443	0.0109
Others (o, f and g)	4.0083	5.832632	7.0538	4.500245
Allobaculum (g)	2.2476	1.3244	3.9467	10.4922
Coprococcus (g)	2.1357	2.2622	0.978	1.9634
Akkermansia (g)	1.1459	0.718	2.9396	1.048
Adlercreutzia (g)	1.076	1.2847	1.9564	2.016
Oscillospira (g)	0.9632	2.4655	1.1927	2.5113
Bacteroides (g)	0.6825	0.4044	0.3086	0.4135
SMB53 (g)	0.4086	2.1813□□□	3.2852♂	1.7301♀
Blautia (g)	0.1732	0.4018	0.2543	0.4719
Desulfovibrio (g)	0.0804	0.2587	2.4434	0.1312
Propionibacterium (g)	0.0421	0.058	0.072	0.1056
Flexispira (g)	0.0351	0.5416	0.2183	0.2797
Erwinia (g)	0.008	0.0038	0.0022	0.0049
Klebsiella (g)	0	0	0	0.0027△♀

Fecal microbiota proportions are shown for bacterial *phyla*, orders, families, and genera in Figs. 3 and 4. WT-M $n = 9$, WT-F $n = 8$, Tg-M $n = 6$, and Tg-F $n = 6$. Data are shown as mean. Statistical significances (*p* values) were calculated by two-way ANOVA with Tukey *post-hoc* correction. Statistical significance between WT-M versus WT-F is shown by □, Tg-M versus Tg-F by ○, WT-M versus Tg-F by △, WT-F versus Tg-M by #, WT-M versus Tg-M by ♂, and WT-F versus Tg-F by ♀; one symbol represents $p < 0.05$, two symbols $p < 0.01$, three symbols $p < 0.001$, and four symbols $p < 0.0001$. f, family; g, genus; o, order; p, *phylum*; Tg-C, transgenic mice fed with control diet; Tg-F, transgenic mice fed with agave fructans supplemented diet; Tg-F-Abx, transgenic mice fed with agave fructans supplemented diet and treated with antibiotics as described in materials and methods; WT-C, wild type mice fed with control diet.

whereas differences for *taxa* enrichment, abundance of sequences related to predictive metabolic pathways and correlations between determined parameters were evidenced by LefSe, t- and one-tailed tests, respectively. All results were considered statistically significant at $p < 0.05$.

RESULTS

Behavioral and cognitive performance

Behavioral tests in female mice were done only at metestrus-/diestrus phase of the estrous cycle.

Anxiety was determined as the proportion of time spent in the open/closed arms in the EPM test. Tg-F mice spent significantly less time in the open arms compared to WT-F, whereas time spent in closed arms was higher in Tg-F compared to WT-M. This data indicates that Tg-F mice showed higher anxiety than their WT-counterpart, which was not observed in males (Fig. 1A, B). Working memory was assessed by the T-maze test. Percentage of spontaneous alternations (%) was higher in WT-F compared to WT-M, Tg-M, and Tg-F mice. WT-M also showed better working memory than Tg-M mice (Fig. 1C). Object
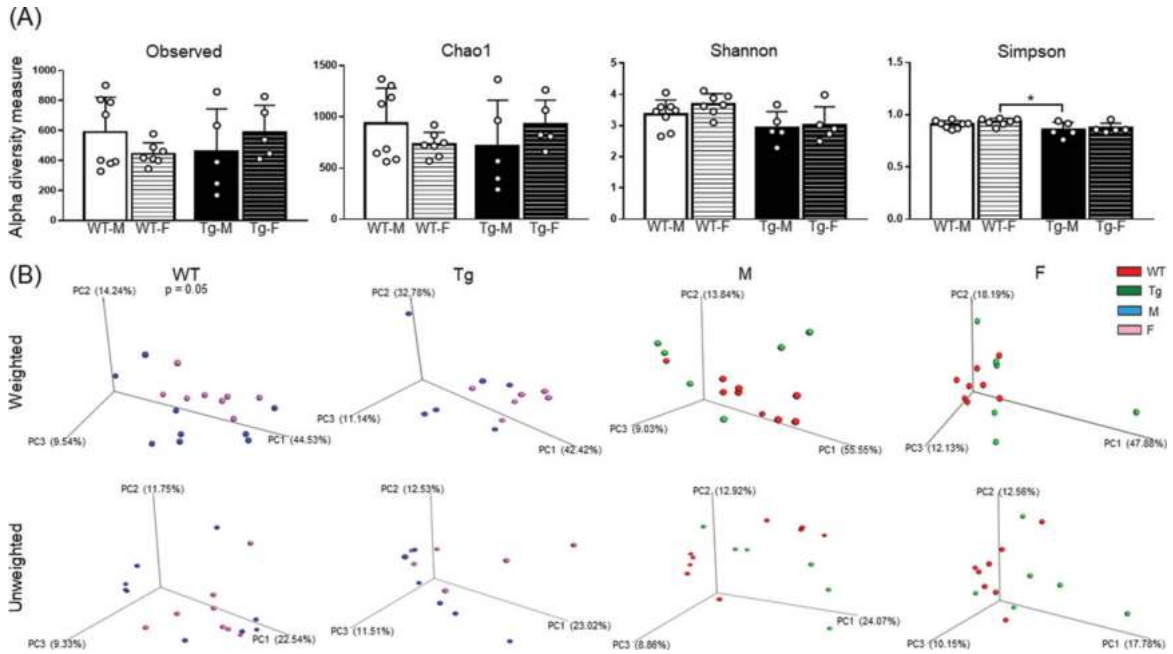
Fig. 4. Fecal microbiota bacterial diversity. Alfa diversity analyses for experimental groups are shown in (A) by observed number of *taxa* [F (1, 21) = 2.71, 0.01 and 0.01 for interaction, row and column factor respectively], Chao1 richness [F (1, 21) = 2.74, 0.0001 and 0.01 for interaction, row and column factor respectively], Shannon index [F (1, 21) = 0.38, 1.19, and 8.02 for interaction, row and column factor respectively] and Simpson index [F (1, 21) = 0.09, 1.15 and 8.65 for interaction, row and column factor respectively]. Beta diversity analyses for experimental groups plotted as principal coordinates analysis (PCoA) in (B) of weighted and unweighted variables. WT-M $n = 9$, WT-F $n = 8$, Tg-M $n = 6$, and Tg-F $n = 6$. For A, white color circles within bars indicate experimental subjects. For B, each subject is represented by a color sphere. Data are shown as mean ± SD bars. For A, data between square brackets indicate F (DFn, DFd) values of two-way ANOVA with Tukey *post-hoc* correction and statistical significances are shown as *$p < 0.05$, **$p < 0.01$, ***$p < 0.001$ and ****$p < 0.0001$. For B, p values for PCoA schemes with significative clustering are showed according to the following results: ADONIS: $R = 0.07$, $p = 0.33$ and ANOSIM: $R = 0.02$, $p = 0.34$ for weighted and ADONIS: $R = 0.10$, $p = 0.05$ and ANOSIM: $R = 0.16$, $p = 0.06$ for unweighted variables comparing WT mice; ADONIS: $R = 0.18$, $p = 0.08$ and ANOSIM: $R = 0.11$, $p = 0.14$ for weighted and ADONIS: $R = 0.09$, $p = 0.47$ and ANOSIM: $R = -0.01$, $p = 0.46$ for unweighted variables comparing Tg mice; ADONIS: $R = 0.10$, $p = 0.18$ and ANOSIM: $R = 0.06$, $p = 0.24$ for weighted and ADONIS: $R = 0.09$, $p = 0.20$ and ANOSIM: $R = 0.11$, $p = 0.14$ for unweighted variables comparing M mice; and ADONIS: $R = 0.10$, $p = 0.23$ and ANOSIM: $R = 0.15$, $p = 0.07$ for weighted and ADONIS: $R = 0.09$, $p = 0.08$ and ANOSIM: $R = 0.26$, $p = 0.01$ for unweighted variables comparing F mice. F, female; M, male; Tg, transgenic; WT, wild type.

Table 2
Alpha diversity indexes for experimental groups

Experimental groups	Statistical parameter	Observed taxa	Chao1 richness	Shannon index	Simpson index
WT (M)		588.63 ± 234.04	933.99 ± 345.31	3.36 ± 0.46	0.91 ± 0.03
WT (F)		443.00 ± 75.09	730.47 ± 118.92	3.68 ± 0.34	0.93 ± 0.03
Tg (M)	mean ± SD	459.80 ± 284.79	717.88 ± 443.44	2.94 ± 0.50	0.86 ± 0.07
Tg (F)		588.20 ± 179.51	924.42 ± 238.42	3.02 ± 0.57	0.87 ± 0.05
WT-M versus WT-F		0.3301	0.3744	0.3461	0.497
Tg-M versus Tg-F	p	0.5512	0.5016	0.9442	0.8584
WT-M versus Tg-M		0.4810	0.3998	0.2393	0.1395
WT-F versus Tg-F		0.4175	0.4921	0.0500	0.0677

Alpha diversity indexes and statistical values for comparisons between WT-M ($n = 9$), WT-F ($n = 8$), Tg-M ($n = 6$), and Tg-F ($n = 6$) mice in Figure 5. Statistical significances (p values) were calculated by two-way ANOVA with Sidak *post-hoc* correction. F, female; M, male; N.A., not applicable; SD, standard deviation; Tg, transgenic mice; WT, wild type mice.

recognition memory was determined by the NOR test. Impaired recognition memory was observed in both Tg-M and Tg-F mice, as they presented lower DIs compared to their WT-counterparts (Fig. 1D).

Spatial-learning and spatial-memory were assessed by the WM test. Learning curves are shown in Fig. 1E. Average time to find the scape platform during all learning trials indicate that Tg-M mice had higher
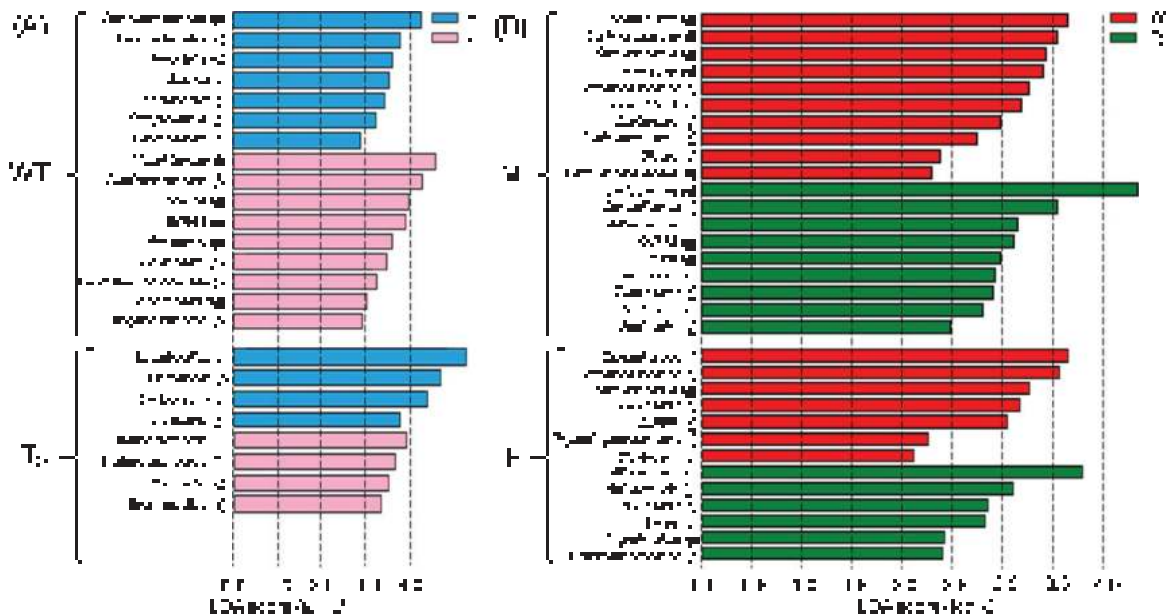
Fig. 5. Fecal enriched bacterial *taxa* associated to gender and genotype. The figure shows the results of the linear discriminant analysis (LDA) effect size (LEfSe) by gender (A) and genotype (B) comparison of differentially abundant bacterial *taxa* (orders, families and genera) significantly associated with WT-M ($n = 9$), WT-F ($n = 8$), Tg-M ($n = 6$), and Tg-F ($n = 6$). For A and B, the color tags on the top right side indicate experimental groups. LDA score (shown at logarithmic scale underneath the bars and indicate with vertical dotted lines) cutoff of 2 was used to discriminate bacterial *taxa*. Specific LDA scores and statistical significances are shown in Supplementary Table 4. F, female; f, family; g, genus; M, male; o, order; Tg, transgenic; WT, wild type.
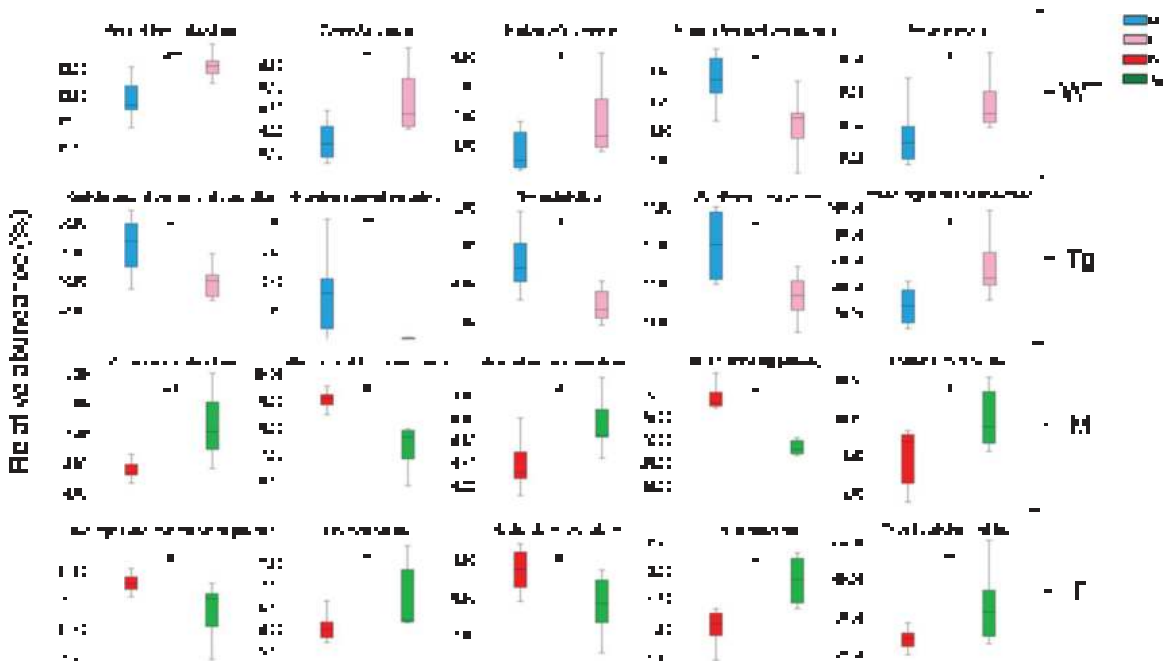

Fig. 6. Prediction of the functional metagenome of the fecal bacterial microbiota. The figure shows graphic representations of significant predicted metabolic pathways determined by PICRUSt v1.1.1 regarding the corresponding bacterial OTU table. Y-axis shows relative abundance to corresponding pathway according to bacterial *taxa* composition for each experimental group (WT-M $n = 9$, WT-F $n = 8$, Tg-M $n = 6$, and Tg-F $n = 6$). Data are shown as mean $\pm$ SD bars. Statistical significances calculated by *t*-test are shown as $^*p < 0.05$, $^{**}p < 0.01$, $^{***}p < 0.001$, and $^{****}p < 0.0001$. F, female; M, male; Tg, transgenic; WT, wild type.
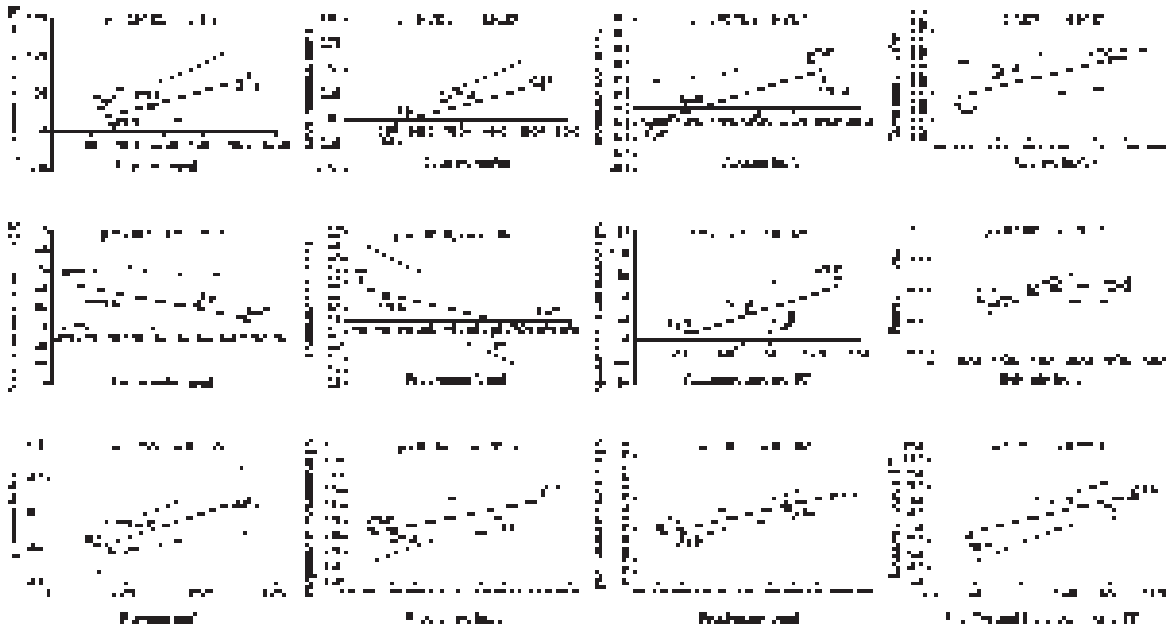
Fig. 7. Correlations between determined parameters. Pearson's correlation between butyrate concentration and spontaneous alternation proportion, butyrate concentration and discrimination index, acetate concentration and discrimination index, acetate concentration and open arm time proportion, propionate concentration and spontaneous alternation proportion, propionate concentration and discrimination index, *Ruminococcaceae* relative abundance and spontaneous alternation proportion, butyrate concentration and Simpson index, butyrate concentration and Shannon index, propionate concentration and propanoate metabolism predicted pathway, propionate concentration and type I diabetes mellitus predicted pathway, and Phe, Tyr and Trp biosynthesis predicted pathway and *Lachnospiraceae* relative abundance are shown. WT-M $n=9$, WT-F $n=8$, Tg-M $n=6$, and Tg-F $n=6$. Data are shown as mean. One-tailed p values (p), Pearson's correlation coefficients (r), trend (solid line) and 95% confidence interval (dotted line) are shown for each correlation. F, female; M, male; Tg, transgenic; WT, wild type.

latencies compared to their WT-counterpart (Fig. 1E, F). To determine effective learning, we compared the latencies to find the scape platform in trial 1 (E1) compared to trial 12 (E12). We observed that only WT mice (both, males and females) were able to show an effective learning as E12 <E1, but Tg mice (both, males and females) did not showed significant differences between E12 and E1 (Fig. 1G). Spatial memory test was carried out after learning trials. WT-F showed better spatial memory than WT-M, Tg-M and Tg-F (Fig. 1H). Representative trajectories during learning and memory phases for M and F subjects are shown in Fig. 1I and 1J, respectively.

Short chain fatty acids concentration

SCFAs were quantified in fecal samples. The concentration of acetate was decreased in Tg mice (male: 14939.03 ± 5496.59 µg/g, female: 11978.96 ± 5480.01 µg/g) compared to their WT counterparts (male: 24776.47 ± 6380.95 µg/g, female: 23768.91 ± 3387.26 µg/g). In contrast, propionate concentration increased in Tg mice (male: 9765.39

± 3128.70 µg/g, female: 7696.35 ± 5746.66 µg/g) compared to their WT counterparts (male: 3056.42 ± 2163.77 µg/g, female: 2071.83 ± 742.01 µg/g). Butyrate concentration was higher in WT-F mice (5263.79 ± 1455.44 µg/g) compared to WT-M (2639.47 ± 1039.08 µg/g), Tg-F (1284.66 ± 432.52 µg/g), and Tg-M mice (1623.90 ± 558.06 µg/g).

Fecal microbiota analysis

To determine whether 6-month-old mice presented sex- and/or genotype-dependent GM dysbiosis, we analyzed the fecal microbiota *taxa* relative abundance in all experimental groups. At *phylum* level, we found a higher abundance of Bacteroidetes in Tg-F compared Tg-M (Figs. 2A and 3, and Table 1). At class level, a higher relative abundance of Bacilli was observed in Tg-M compared to Tg-F (Fig. 3, Supplementary Figure 1, and Supplementary Table 3). At order level, higher abundances of Lactobacillales and Turicibacterales were observed in Tg-M compared to Tg-F mice and compared to WT-F only for Turicibacterales (Fig. 3, Table 1, Supplementary

Figure 1, and Supplementary Table 3). At family level, *Clostridiaceae* abundance was higher in WT-F compared to WT-M mice. *Lactobacillaceae* relative abundance was higher in Tg-M compared to the rest of the groups. *S24-7* showed an increase in Tg-F compared to Tg-M, and *Turicibacteraceae* was higher in Tg-M compared to Tg-F and WT-F (Fig. 3, Table 1, Supplementary Figure 1, and Supplementary Table 3). At genus level, abundance of *Klebsiella* was higher in Tg-F compared to WT-F and WT-M, while *Lactobacillus* was higher in Tg-M compared to Tg-F. *Lactococcus* showed higher proportions in Tg-M compared to the other three groups, and *SMB53* showed a higher abundance in WT-F compared to WT-M and Tg-F, increasing its abundance in Tg-M in comparison to WT-M mice (Figs. 2B and 3 and Table 1).

Alpha diversity was estimated by the Observed number of *taxa*, Chao1 richness and Shannon and Simpson indexes (rarefaction curves are shown in Supplementary Figure 2). A decreased bacterial diversity was observed in Tg-M compared to WT-F according to Simpson index (Fig. 4A). No significant differences were found in observed number of *taxa*, Chao1 richness and Shannon index (Table 2). The clustering the bacterial communities using PCoA of weighted and unweighted variables revealed a sex-dependent segregation between WT mice comparing weighted variables, without statistical clustering for the rest of comparisons (Fig. 4B).

Next, we used a linear discriminant analysis effect size (LEfSe) to determine enriched *taxa* per condition. Seven *taxa* were enriched in WT-M versus WT-F (*Stenotrophomonas, Parabacteroides, Prevotella, Slackia, Acetobacter, Paraprevotella* and *Coprobacillus*), whereas nine *taxa* were enriched in WT-F versus WT-M (*Clostridiaceae, Ruminococcaceae, SMB53, EW055, Fusibacter, Flexispira, Peptostreptococcaceae, Kaistobacter* and *Mogibacteriaceae*). Additionally, four *taxa* were enriched in Tg-M versus to Tg-F (*Lactobacillus*, Dietziaceae, *Lactococcus* and *Variovorax*) and four in Tg-F versus Tg-M (*Koribacteraceae, Erythrobacteraceae, Koribacter* and Stramenopiles) (Fig. 5A and Supplementary Table 4). Also, ten *taxa* were enriched for WT-M versus Tg-M (*Allobaculum*, Lachnospiraceae, *Ruminococcus*, *Nitrospira*, *Ruminococcaceae*, *Coprococcus*, *Oscillospira*, *Lachnobacterium*, *Blautia* and *Christiansenellaceae*), whereas nine *taxa* were enriched in Tg-M versus WT-M (*Lactobacillus*, Clostridiaceae, *Adlercreutzia*, *SMB53*, *Dorea*, *Variovorax*, *Turicibacter*, *Clostridium* and *Fusibacter*). Regarding

females, seven *taxa* were enriched in WT-F versus Tg-F (Clostridiaceae, Ruminococcaceae, *Ruminococcus, Fusibacter*, *SMB53*, *Peptostreptococcaceae*, and *Clostridium*), while six enriched *taxa* were observed in Tg-F versus WT-F (*Allobaculum, Adlercreutzia, Koribacter, Dorea, Coprobacillus* and *Christiansenellaceae*; Fig. 5B and Supplementary Table 4).

Metagenome prediction analysis

Functional metabolic pathways related to fecal microbiota abundances was determined by PICRUSt analysis using the OTU table. The main 20 pathways showing statistically significant difference between experimental groups were mostly linked with metabolism, genetic information processing, human diseases, organismal systems, and environmental information processing (Fig. 6 and Supplementary Table 5). Among these, arginine (Arg) and proline (Pro) metabolism, colorectal cancer, Parkinson's disease, and toxoplasmosis were increased in WT-F with respect to WT-M, while primary bile acid biosynthesis was decreased in WT-F regarding WT-M. On the other hand, carbohydrate digestion and absorption, G protein-coupled receptors, tyrosine (Tyr), and glutathione metabolism were decreased in Tg-F in comparison to Tg-M mice. Protein digestion and absorption was decreased in Tg-M compared to Tg-F. Tg-M presented increases in propanoate, arachidonic acid and pyruvate metabolic related-pathways, and decreases in insulin signaling pathway and phenylalanine (Phe), Tyr and tryptophan (Trp) biosynthesis compared to WT-M. On the other hand, Tg-F presented increases in type I diabetes mellitus and histidine (His) and Trp metabolism, and decreases in naphthalene degradation, DNA repair, and recombination proteins compared to WT-F (Fig. 6).

Correlations analysis

The determine the possible association between behavioral/cognitive performance in the experimental groups versus SCFAs concentration, *taxa* relative abundance, alpha diversity metrics, and predicted metabolic pathways we used the Pearson's correlation coefficient test (Fig. 7). Butyrate concentrations correlated positively with working- and object recognition memory with the highest values in WT-F mice, and the lowest in Tg-F mice. Acetate concentration correlated positively with a better object recognition memory and with lower anxiety index,

as WT mice showed the higher values and Tg-F mice the lower values. Propionate levels in fecal samples showed a negative correlation with working memory and object-recognition memory, as Tg-M mice showed the highest values. Among all detected *taxa*, only *Ruminococcaceae* and *Lachnospiraceae* families were positively correlated with working memory and Phe, Tyr, and Trp biosynthesis predicted pathway, respectively. Simpson and Shannon indexes were positively correlated with butyrate concentrations, with highest values found in WT-F mice. Finally, propionate concentrations in feces were positively correlated with propanoate metabolism, and Type I diabetes mellitus predicted pathways, with highest values in Tg-M mice (Fig. 7).

DISCUSSION

The higher risk for women to develop AD has been associated with a decline in sex hormones during the transition to the menopause [5, 6]. However, brain alterations can be observed even before menopause [69, 70], despite ovarian estrogen production and an active reproductive function. Therefore, it remains to be explained why women are at higher risk to develop AD than men. Here, we aimed to describe whether GM alterations can be associated with the cognitive decline in 6-month-old APP/PS1 mice (Tg) based on a sex/genotype segregation design. We observed sex-dependent differences in cognitive skills in male versus female WT mice, favoring females. However, in Tg-F mice the cognitive advantage over males was lost. GM composition showed few differences between female and male WT mice, with only a marked abundance of *Clostridiaceae* in WT-F compared to their opposite sex. Tg mice showed several sex-dependent GM alterations, being more pronounced in male mice. In addition, Tg mice showed decreased concentrations of butyrate and acetate compared to sex-matched WT mice. However, propionate was highly abundant in Tg mice (both sexes) compared to their sex-matched controls. Butyrate and acetate levels were directly associated with better working- and object recognition memory. Contrary, propionate was inversely associated with those types of memories.

For this work, we used APP/PS1 mice as they develop spatial, working, and recognition memory impairments starting at 3-4 months of age [71, 72]. In addition, APP/PS1 mice also presented detectable GM alterations since three months of age [73], being

more pronounced after six months of age compared to WT animals [74–78]. Thus, APP/PS1 mice are an ideal AD model to evaluate dysbiosis-related to memory alterations.

The first objective of our study was to describe sex-dependent cognitive alterations in WT and Tg mice. In AD mice models, it has been shown that male and female 3xTgAD mice presented equally impaired cognition at 4 months of age and a faster rate of cognitive decline in females compared to male mice at 9 months of age, but this sex-differences were lost at 12 months of age, as both sexes performed worse than their WT counterparts [34]. We observed a better working memory in WT-F compared to WT-M mice in the T-maze test. However, this sexual dimorphism disappeared in Tg mice, as both male and females Tg mice showed similar percentage of spontaneous alternations and an impaired spatial learning compared to WT mice. APP/PS1 mice model develops neuropathological and cognitive alterations early than the previously used 3xTgAD mice. Therefore, our data supports early studies in humans and Tg models where sexual dimorphism in healthy subjects (WT) favors females, while AD pathology abates the sexual dimorphism in cognition.

The pathological hallmarks of AD also showed a sexual dimorphism that is present in young and old Tg mice as females exhibit an increased plaque burden and higher $A\beta_{40}$ levels than age-matched males along aging [31–33]. Notwithstanding, female Tg mice do not show worst cognitive impairment as amyloid pathology progresses, compared to males. Previous studies addressed the concept of compensatory mechanisms against brain dysfunction during the perimenopausal period in females. Perimenopause is characterized by brain alterations such as a decline in glucose metabolism and neuronal bioenergetics [79, 80], allowing a better utilization of ketone bodies as an alternative brain fuel [70, 81, 82]. Those compensatory mechanism are observed around 6–9 months of age in healthy mice, but as early as 3 months in Tg mice [80]. Notably, peripheral metabolic alterations are also observed in perimenopause rodents [79, 80, 83]. GM composition has important role in host-metabolism, and dysbiosis has been associated with obesity and diabetes onset [84–86]. In this study, we did not measure brain or peripheral bioenergetics markers. However, our predicted metabolic pathway showed that Tg-F mice has an enhanced metabolic pathway linked to diabetes type-1 than WT-F, that may reflect an impaired peripheral glucose metabolism.

Recent focus has been paid to GM alterations and their possible impact in brain function. AD patients show an altered GM composition compared to healthy age-matched subjects [41–46]. However, those previous reports did not discriminate between genders. Cox et al. (2019) showed more age-related microbiome changes in female Tg mice (Tg2576) compared to female WT mice [87]. Importantly, GM alterations in Tg mice can be already detected since the first and third month of age compared to their WT littermates, preceding brain amyloid-β aggregation [73]. The impact of GM on the neuropathological hallmarks of AD was demonstrated in germ-free Tg mice and antibiotic-treated Tg mice, as under both experimental conditions Tg mice showed a reduction in brain amyloid-β aggregation in male mice [75, 76]. However, similar antibiotic treatment did not affect amyloid-β aggregation in female Tg mice [47]. This females' antibiotic resistant effect abating amyloid aggregation may have important implications in the etiology of AD. Our data showed a lower GM diversity trend in Shannon and Simpson indexes for Tg-F compared to WT-F group. Similarly, AD patients show lower microbial diversity compared to healthy controls [45]. We did not observe significant differences at *phylum* level between WT and Tg mice. However, at a more specific level of *taxa*, several differences were detected between Tg-F and Tg-M mice, while a more homogeneous ecology was observed between WT-M and WT-F mice. In the one side, WT-F show an increased abundance of *Clostridiaceace* compared to WT-M. On the other side, Tg-M mice presented an increased abundance of Bacilli (class), Lactobacillales, Turicibacterales (orders), *Lactobacillaceae, Turicibacteraceae* (families), *Lactobacillus*, and *Lactococcus* (genera) compared to Tg-F mice. Meanwhile, Tg-F showed an enhanced abundance of Bacteroidetes (*phylum*), *S24-7* (family), and *Klebsiella* (genus) compared to Tg-M mice. *Turibacteraceae* is a bacteria linked to inflammatory conditions [88], and *Lactococcus*, an acid lactic producing bacteria [89], has been associated with cognitive dysfunction and neurological impairment [90]. Sex-dependent expression of neuroinflammation markers have been reported in humans [91] and mice [92] with aging, with a more exacerbated response in females. It remains to be explored whether GM dysbiosis in Tg-F mice may initiate a stronger inflammatory reaction compared to their males counterparts at six months of age.

When comparing GM composition between WT-F and Tg-F, we observed an increased abundance of *Ruminococcaceae* and *Clostridiaceae* WT-F mice. *Ruminococcaceae* and *Clostridiales* have been associated with higher circulating estrogens levels in postmenopausal women [93]. Correlation analysis raveled a positive association between *Ruminococcaceae* and working memory, with highest values in WT-F. WT-F mice also presented an enrichment of *Clostridiaceae* and *Clostridium* compared to Tg-F mice. The presence of those gut bacteria may have important consequences in estrogen bioavailability. Regretfully, we did not measure serum estrogen levels in these animals.

The effect size analysis (LEfSe) by sex and genotype showed substantial differences between groups. *Allobaculum, Adlercreuzia, Koribacter*, and *Dorea* were enriched in Tg-F mice compared to WT-F. Increased abundances of *Allobaculum* is considered a risk factor of female hepatocellular carcinoma [94]. In addition, mucin degradation and gut-barrier dysfunction have been associated with higher *Dorea* abundance [95] in alcohol-dependent subjects [96], and certain species of *Dorea* promote IFNγ production and chronic inflammation in multiple-sclerosis patients [97]. Tg-M showed significant enrichment of *Lactobacillus*, *Clostridiaceae*, *Adlercreutzia*, *SMB53*, *Dorea*, *Variovorax*, *Turicibacter, Clostridium*, and *Fusibacter*, compared to WT-M. *Clostridium butyricum* has showed neuroprotective effects [98, 99]. Contrastingly, *Clostridium* type-structures have been detected by immunohistochemistry in AD brain tissue [100]. Thus, our data showed that Tg-M suffer a more severe GM dysbiosis compared to Tg-F mice.

One relevant data collected in this study was the genotype-dependent alterations in bacterial fermented products such as SCFAs. We observed an enhanced propionate, but a reduced butyrate concentration in Tg mice (male and female) compared to their WT-counterparts. Increased propionate and acetate levels have been found in saliva of AD patients [101, 102], indicating that microbiota dysbiosis in AD is not restricted to the gut. We previously reported a prominent abundance of *Prevotella copri*, a propionate producing bacteria, in fecal samples of another Tg mice model (3xTgAD), that was associated with an enhanced propionate concentration in Tg brain tissue compared to the control mice [56]. Here, we also observed a significant increase in propionate producing bacteria in Tg-M mice, such as *Lactobacillus* (propionate producing species: *L. buchneri*, *L. dioliivorans*, *L. acidophilus*, *L. helviticus, L. rhamnosus*, and *L.* gasseri) [103–105]. Previous studies also

reported a *Lactobacillus* enrichment in fecal samples of male Tg mice [106, 107] and AD patients [108]. *Lactobacilli* are often considered to be commensal or beneficial participants to the host microbial ecology; however, they have been identified as potential pathogens in elderly and immunocompromised patients [109, 110]. In addition, patients with myalgic encephalomyelitis/chronic fatigue syndrome present a direct correlation between *Lactobacillus* distribution and symptom, neurocognitive, and neurosensory factors associated with neurological impairment [111]. Thus, caution may be taken for future probiotic design and supplementation protocols for AD patients. In addition, Tg mice (both, males and females) also presented a significant reduction in butyrate-producing bacteria (e.g., Lachnospiraceae, Ruminococcaceae, Peptostreptococcaceae, and *Oscillospira*) and acetate-producing bacteria (*Blautia*, Christiansenellaceaea, and *Ruminococcus* [43, 112–117]. Previous investigations have reported a general reduction in SCFAs concentration in brain and fecal samples of APP/PS1 mice [77]. However, significant biological differences among the principal bacterial fermented products have been described. Intracerebroventricular infusion of propionate in rats results in neuroinflammation [118, 119], progressive development of limbic kindled seizures, oxidative stress (e.g.,

lipid peroxidation), microglial activation-associated with decreased glutathione activity [120], and impairments in social behavior and working memory [121]. In the present study, WT-F mice presented an increase in butyrate-producing *taxa* (i.e., *Clostridiaceae*) compared to Tg-F, and highest butyrate concentration compared to the other groups. Correlation analysis further indicates that butyrate concentration correlates positively with working- and object-recognition memory, while propionate concentrations had a negative correlation with those memory capabilities. Sodium butyrate treatment protect against cerebral Ischemia [99], improving associative memory in APP/PS1 mice even at an advance stage of the disease [122]. Moreover, butyrate suppresses microglia activation [123] and decreases astrocyte activation [124] in cell cultures. Therefore, our results may indicate that Tg mice lack several butyrate-producing bacteria, with important neuroprotective effects, but they carry specific gut bacteria capable of releasing neurotoxic substances (i.e., propionate).

Predicted metabolic pathways of the fecal bacterial microbiota by functional metagenome indicate that GM modulation by genotype and gender is related to different bacterial products that interact with the host-physiology. We observed an enhanced propanoate metabolism pathway in Tg-M that could also be associated with *Lactobacillus* abundance
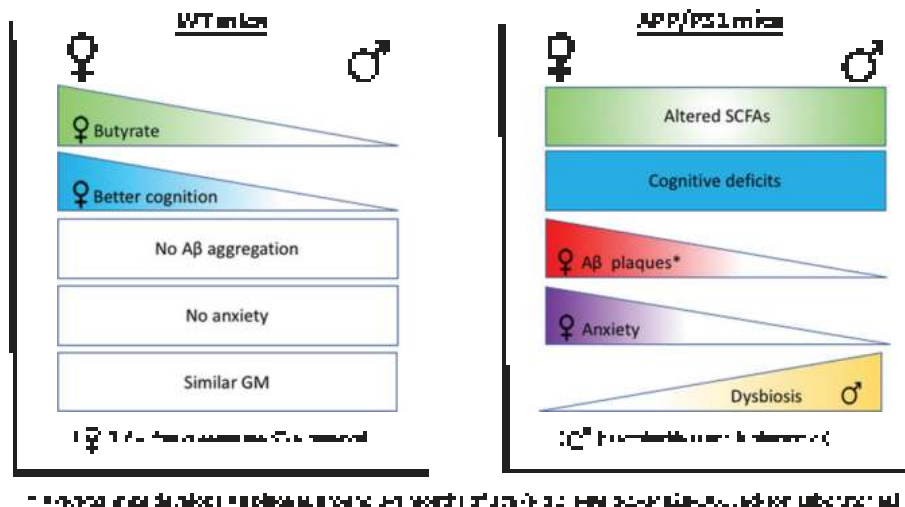

Fig. 8. Graphical abstract: WT-F mice showed higher butyrate concentration in fecal samples, which was associated with better cognitive performance compared WT-M and Tg-F mice. WT mice (without Aβ aggregates) did not showed anxiety. WT-F and WT-M mice present similar GM composition Notably, WT-F mice presented an enrichment of *Ruminococcaceae* and *Clostridiales* compared to Tg-F mice. APP/PS1 (Tg) mice (that develop Aβ plaques), showed altered short-chain-fatty acids (SCFAs) concentration (lower acetate/butyrate, but higher propionate) compared to their WT counterparts, cognitive deficits, and enhanced anxiety compared to WT mice. GM dysbiosis was stronger in Tg-M than Tg-F. Tg-M showed enrichment of *Lactobacillaceae* and *Turicibacteraceae* compared to WT-M and Tg-F mice.

and fecal propionate levels in this group. Protein digestion and absorption were increased in Tg-F compared to Tg-M mice. A recent study showed a reduced protein digestion and absorption pathway in APPPS1-21 mice treated with antibiotics (both, female and male animals) [47]. Our study, based in a sex-discrimination analysis, showed that this metabolic pathway was reduced in Tg-M compared to Tg-F mice. The PICRUSt analysis also revealed a reduced Phe, Tyr, and Trp pathway in Tg-M mice compared to their WT counterparts. Low concentrations of Phe, Tyr, and Trp have been found in AD patients compared to control individuals [125], and lower Trp and kynurenic acid plasma concentrations were correlated with dementia severity in AD patients [126]. Thus, the collected data may indicate that several metabolic and cellular alterations observed in AD patients and Tg mice can be associated with GM dysbiosis.

In conclusion, this study shows a direct association among GM, cognitive decline, and sexual dimorphism in an AD mice model (Fig. 8). Sex differences in GM composition were observed mainly in Tg mice, which implies that sex itself exerted specific influences on the composition of the microbiota in AD pathology. The changes in composition of the GM between male and female Tg mice, and its physiological implications may be related with the dimorphism observed in the incidence of AD, affecting more women than men. Further studies are needed to understand the impact of female Tg dysbiosis in AD pathology, and to explore whether specific taxa may confer protection against brain dysfunction.

ACKNOWLEDGMENTS

SUPPLEMENTARY MATERIAL

The supplementary material is available in the electronic version of this article: https://dx.doi.org/10.3233/JAD-201367.

REFERENCES

[1] Alzheimer Association (2020) Alzheimer's disease facts and figures. *Alzheimers Dement* **16**, 391-460.

[2] Livingston G, Sommerlad A, Orgeta V, Costafreda SG, Huntley J, Ames D, Ballard C, Banerjee S, Burns A, Cohen-Mansfield J, Cooper C, Fox N, Gitlin LN, Howard R, Kales HC, Larson EB, Ritchie K, Rockwood K, Sampson EL, Samus Q, Schneider LS, Selbæk G, Teri L, Mukadam N (2017) Dementia prevention, intervention, and care. *Lancet* **390**, 2673-2734.

[3] Scheyer O, Rahman A, Hristov H, Berkowitz C, Isaacson RS, Diaz Brinton R, Mosconi L (2018) Female sex and Alzheimer's risk: The menopause connection. *J Prev Alzheimers Dis* **5**, 225-230.

[4] Alzheimer Association (2019) Alzheimer's disease facts and figures. *Alzheimers Assoc* **15**, 321-387.

[5] Gilsanz P, Lee C, Corrada MM, Kawas CH, Quesenberry CP, Whitmer RA (2019) Reproductive period and risk of dementia in a diverse cohort of health care members. *Neurology* **92**, e2005-e2014.

[6] Fox M, Berzuini C, Knapp LA (2013) Cumulative estrogen exposure, number of menstrual cycles, and Alzheimer's risk in a cohort of British women. *Psychoneuroendocrinology* **38**, 2973-2982.

[7] Yamada M, Landes RD, Mimori Y, Nagano Y, Sasaki H (2015) Trajectories of cognitive function in dementia-free subjects: Radiation Effects Research Foundation Adult Health Study. *J Neurol Sci* **351**, 115-119.

[8] Eals M, Silverman I (1994) The hunter-gatherer theory of spatial sex differences: Proximate factors mediating the female advantage in recall of object arrays. *Ethol Sociobiol* **15**, 95-105.

[9] McBurney DH, Gaulin SJC, Deviveni T, Adams C (1997) Superior spatial memory of women: Stronger evidence for the gathering hypothesis. *Evol Hum Behav* **18**, 165-174.

[10] Galea LAM, Kimura D (1993) Sex differences in route-learning. *Pers Individ Dif* **14**, 53-65.

[11] Harshman RA, Hampson E, Berenbaum SA (1983) Individual differences in cognitive abilities and brain organization, part I: Sex and handedness differences in ability. *Can J Psychol* **37**, 144-192.

[12] Peters A, Josephson K, Vincent SL (1991) Effects of aging on the neuroglial cells and pericytes within area 17 of the rhesus monkey cerebral cortex. *Anat Rec* **229**, 384-398.

[13] Voyer D, Voyer S, Bryden MP (1995) Magnitude of sex differences in spatial abilities: A meta-analysis and consideration of critical variables. *Psychol Bull* **117**, 250-270.

[14] Parsons TD, Rizzo AR, Van Der Zaag C, McGee JS, Buckwalter JG (2005) Gender differences and cognition among older adults. *Aging Neuropsychol Cogn* **12**, 78-88.

[15] Savage RM, Gouvier WD (1992) Rey auditory-verbal learning test: The effects of age and gender, and norms for delayed recall and story recognition trials. *Arch Clin Neuropsychol* **7**, 407-414.

[16] Laws K, Irvine K, Gale T (2016) Sex differences in cognitive impairment in Alzheimer's disease. *World J Psychiatry* **6**, 54-65.

[17] Wiederholt WC, Cahn D, Butters NM, Salmon DP, Kritz-Silverstein D, Barrett-Connor E (1993) Effects of age, gender and education on selected neuropsychological tests in an elderly community cohort. *J Am Geriatr Soc* **41**, 639-647.

[18] Maylor EA, Reimers S, Choi J, Collaer ML, Peters M, Silverman I (2007) Gender and sexual orientation differences in cognition across adulthood: Age is kinder to women than to men regardless of sexual orientation. *Arch Sex Behav* **36**, 235-249.

[19] Read S, Pedersen NL, Gatz M, Berg S, Vuoksimaa E, Malmberg B, Johansson B, McClearn GE (2006) Sex differences after all those years? Heritability of cognitive abilities in old age. *J Gerontol B Psychol Sci Soc Sci* **61**, P137-P143.

[20] Proust-Lima C, Amieva H, Letenneur L, Orgogozo J-M, Jacqmin-Gadda H, Dartigues JF (2008) Gender and education impact on brain aging: A general cognitive factor approach. *Psychol Aging* **23**, 608-620.

[21] Gerstorf D, Herlitz A, Smith J (2006) Stability of sex differences in cognition in advanced old age: The role of education and attrition. *J Gerontol B Psychol Sci Soc Sci* **61**, P245-P249.

[22] Sundermann EE, Maki PM, Rubin LH, Lipton RB, Landau S, Biegon A; Alzheimer's Disease Neuroimaging Initiative (2016) Female advantage in verbal memory: Evidence of sex-specific cognitive reserve. *Neurology* **87**, 1916-1924.

[23] Sundermann EE, Biegon A, Rubin LH, Lipton RB, Mowrey W, Landau S, Maki PM; Alzheimer's Disease Neuroimaging Initiative (2016) Better verbal memory in women than men in MCI despite similar levels of hippocampal atrophy. *Neurology* **86**, 1368-1376.

[24] Sundermann EE, Biegon A, Rubin LH, Lipton RB, Landau S, Maki PM; Alzheimer's Disease Neuroimaging Initiative (2017) Does the female advantage in verbal memory contribute to underestimating Alzheimer's disease pathology in women versus men? *J Alzheimers Dis* **56**, 947-957.

[25] Chapman RM, Mapstone M, Gardner MN, Sandoval TC, McCrary JW, Guillily MD, Reilly LA, DeGrush E (2011) Women have farther to fall: Gender differences between normal elderly and Alzheimer's disease in verbal memory engender better detection of Alzheimer's disease in women. *J Int Neuropsychol Soc* **17**, 654-662.

[26] Beinhoff U, Tumani H, Brettschneider J, Bittner D, Riepe MW (2008) Gender-specificities in Alzheimer's disease and mild cognitive impairment. *J Neurol* **255**, 117-122.

[27] Buckwalter JG, Rizzo AA, McCleary R, Shankle R, Dick M, Henderson VW (1996) Gender comparisons of cognitive performances among vascular dementia, Alzheimer disease, and older adults without dementia. *Arch Neurol* **53**, 436-439.

[28] Heun R, Kockler M (2002) Gender differences in the cognitive impairment in Alzheimer's disease. *Arch Womens Ment Health* **4**, 129-137.

[29] Barnes LL, Wilson RS, Bienias JL, Schneider JA, Evans DA, Bennett DA (2005) Sex differences in the clinical manifestations of Alzheimer disease pathology. *Arch Gen Psychiatry* **62**, 685-691.

[30] Sandberg G, Stewart W, Smialek J, Troncoso JC (2001) The prevalence of the neuropathological lesions of Alzheimer's disease is independent of race and gender. *Neurobiol Aging* **22**, 169-175.

[31] Callahan MJ, Lipinski WJ, Bian F, Durham RA, Pack A, Walker LC (2001) Augmented senile plaque load in aged female β-amyloid precursor protein-transgenic mice. *Am J Pathol* **158**, 1173-1177.

[32] Wang J, Tanila H, Puoliväli J, Kadish I, van Groen T (2003) Gender differences in the amount and deposition of amyloidβ in APPswe and PS1 double transgenic mice. *Neurobiol Dis* **14**, 318-327.

[33] Jiao SS, Bu X Le, Liu YH, Zhu C, Wang QH, Shen LL, Liu CH, Wang YR, Yao XQ, Wang YJ (2016) Sex dimorphism profile of Alzheimer's disease-type pathologies in an APP/PS1 mouse model. *Neurotox Res* **29**, 256-266.

[34] Clinton LK, Billings LM, Green KN, Caccamo A, Ngo J, Oddo S, McGaugh JL, LaFerla FM (2007) Age-dependent sexual dimorphism in cognition and stress response in the 3xTg-AD mice. *Neurobiol Dis* **28**, 76-82.

[35] Jiang C, Li G, Huang P, Liu Z, Zhao B (2017) The gut microbiota and Alzheimer's disease. *J Alzheimers Dis* **58**, 1-15.

[36] Lyte M, Cryan JF (2014) *Microbial Endocrinology: The Microbiota-Gut-Brain Axis in Health and Disease.* Springer.

[37] Reveles KR, Patel S, Forney L, Ross CN (2019) Age-related changes in the marmoset gut microbiome. *Am J Primatol* **81**, e22960.

[38] Lee SM, Kim N, Park JH, Nam RH, Yoon K, Lee DH (2018) comparative analysis of ileal and cecal microbiota in aged rats. *J Cancer Prev* **23**, 70-76.

[39] Biagi E, Nylund L, Candela M, Ostan R, Bucci L, Pini E, Nikkïla J, Monti D, Satokari R, Franceschi C, Brigidi P, De Vos W (2010) Through ageing, and beyond: Gut microbiota and inflammatory status in seniors and centenarians. *PLoS One* **5**, e10667.

[40] Biagi E, Franceschi C, Rampelli S, Severgnini M, Ostan R, Turroni S, Consolandi C, Quercia S, Scurti M, Monti D, Capri M, Brigidi P, Candela M (2016) Gut microbiota and extreme longevity. *Curr Biol* **26**, 1480-1485.

[41] Cattaneo A, Cattane N, Galluzzi S, Provasi S, Lopizzo N, Festari C, Ferrari C, Guerra UP, Paghera B, Muscio C, Bianchetti A, Volta GD, Turla M, Cotelli MS, Gennuso M, Prelle A, Zanetti O, Lussignoli G, Mirabile D, Bellandi D, Gentile S, Belotti G, Villani D, Harach T, Bolmont T, Padovani A, Boccardi M, Frisoni GB; INDIA-FBP Group (2017) Association of brain amyloidosis with pro-inflammatory gut bacterial taxa and peripheral inflammation markers in cognitively impaired elderly. *Neurobiol Aging* **49**, 60-68.

[42] Haran JP, Bhattarai SK, Foley SE, Dutta P, Ward DV, Bucci V, McCormick BA (2019) Alzheimer's disease microbiome is associated with dysregulation of the anti-inflammatory p-glycoprotein pathway. *mBio* **10**, e00632-19.

[43] Liu P, Wu L, Peng G, Han Y, Tang R, Ge J, Zhang L, Jia L, Yue S, Zhou K, Li L, Luo B, Wang B (2019) Altered microbiomes distinguish Alzheimer's disease from amnestic mild cognitive impairment and health in a Chinese cohort. *Brain Behav Immun* **80**, 633-643.

[44] Li B, He Y, Ma J, Huang P, Du J, Cao L, Wang Y, Xiao Q, Tang H, Chen S (2019) Mild cognitive impairment has similar alterations as Alzheimer's disease in gut microbiota. *Alzheimers Dement* **15**, 1357-1366.

[45] Vogt NM, Kerby RL, Dill-McFarland KA, Harding SJ, Merluzzi AP, Johnson SC, Carlsson CM, Asthana S, Zetterberg H, Blennow K, Bendlin BB, Rey FE (2017) Gut microbiome alterations in Alzheimer's disease. *Sci Rep* **7**, 13537.

[46] Zhuang ZQ, Shen LL, Li WW, Fu X, Zeng F, Gui L, Lü Y, Cai M, Zhu C, Tan YL, Zheng P, Li HY, Zhu J, Zhou HD, Bu XL, Wang YJ (2018) Gut microbiota is altered in patients with Alzheimer's disease. *J Alzheimers Dis* **63**, 1337-1346.

[47] Dodiya HB, Kuntz T, Shaik SM, Baufeld C, Leibowitz J, Zhang X, Gottel N, Zhang X, Butovsky O, Gilbert JA, Sisodia SS (2019) Sex-specific effects of microbiome perturbations on cerebral Ab amyloidosis and microglia phenotypes. *J Exp Med* **216**, 1542-1560.

[48] Reeves PG, Nielsen FH, Fahey GC Jr (1993) Ain-93 purified diets for laboratory rodents - final report of the American Institute of Nutrition Ad Hoc Writing Committee on the reformulation of the Ain-76a rodent diet. *J Nutr* **123**, 1939-1951.

[49] Miller BH, Takahashi JS (2014) Central circadian control of female reproductive function. *Front Endocrinol (Lausanne)* **4**, 195.

[50] Walf AA, Frye CA (2007) The use of the elevated plus maze as an assay of anxiety-related behavior in rodents. *Nat Protoc* **2**, 322-328.

[51] Byers SL, Wiles MV, Dunn SL, Taft RA (2012) Mouse estrous cycle identification tool and images. *PLoS One* **7**, e35538.

[52] Caligioni C (2009) Assessing reproductive status/stages in mice. *Curr Protoc Neurosci* APPENDIX: Appendix-4I. doi:10.1002/0471142301.nsa04is48.

[53] Deacon RM, Rawlins JN (2006) T-maze alternation in the rodent. *Nat Protoc* **1**, 7-12.

[54] Gerlai R (1998) A new continuous alternation task in T-maze detects hippocampal dysfuncion in mice. A strain comparison and lesion study. *Behav Brain Res* **95**, 91-101.

[55] Davis KE, Burnett K, Gigg J (2017) Water and T-maze protocols are equally efficient methods to assess spatial memory in 3xTg Alzheimer's disease mice. *Behav Brain Res* **331**, 54-66.

[56] Syeda T, Sanchez-Tapia M, Pinedo-Vargas L, Granados O, Cuervo-Zanatta D, Rojas-Santiago E, Díaz-Cintra S, Torres N, Perez-Cruz C (2018) Bioactive food abates metabolic and synaptic alterations by modulation of the brain-gut axis in a mouse model of Alzheimer's disease. *J Alzheimers Dis* **66**, 1657-1682.

[57] Moojen VK, Damiani-Neves M, Bavaresco DV, Pescador BB, Comim CM, Quevedo J, Boeck CR (2012) NMDA preconditioning prevents object recognition memory impairment and increases brain viability in mice exposed to traumatic brain injury. *Brain Res* **1466**, 82-90.

[58] Bird CM (2017) The role of the hippocampus in recognition memory. *Cortex* **93**, 155-165.

[59] Morici JF, Bekinschtein P, Weisstaub NV (2015) Medial prefrontal cortex role in recognition memory in rodents. *Behav Brain Res* **292**, 241-251.

[60] Nunez J (2008) Morris water maze experiment. *J Vis Exp* **897**, doi: 10.3791/897.

[61] Sharma S, Rakoczy S, Brown-Borg H (2010) Assessment of spatial memory in mice. *Life Sci* **87**, 521-536.

[62] Binder S, Mölle M, Lippert M, Bruder R, Aksamaz S, Ohl F, Wiegert JS, Marshall L (2019) Monosynaptic hippocampal-prefrontal projections contribute to spatial memory consolidation in mice. *J Neurosci* **39**, 6978-6991.

[63] Murugesan S, Ulloa-Martínez M, Martínez-Rojano H, Galván-Rodríguez FM, Miranda-Brito C, Romano MC, Piña-Escobedo A, Pizano-Zárate ML, Hoyo-Vadillo C, García-Mena J (2015) Study of the diversity and short-

chain fatty acids production by the bacterial community in overweight and obese Mexican children. *Eur J Clin Microbiol Infect Dis* **34**, 1337-1346.

[64] De Baere S, Eeckhaut V, Steppe M, De Maesschalck C, De Backer P, Van Immerseel F, Croubels S (2013) Development of a HPLC-UV method for the quantitative determination of four short-chain fatty acids and lactic acid produced by intestinal bacteria during *in vitro* fermentation. *J Pharm Biomed Anal* **80**, 107-115.

[65] Corona-Cervantes K, García-González I, Villalobos-Flores LE, Hernández-Quiroz F, Piña-Escobedo A, Hoyo-Vadillo C, Rangel-Calvillo MN, García-Mena J (2020) Human milk microbiota associated with early colonization of the neonatal gut in Mexican newborns. *PeerJ* **8**, e9205.

[66] Caporaso JG, Kuczynski J, Stombaugh J, Bittinger K, Bushman FD, Costello EK, Fierer N, Peña AG, Goodrich JK, Gordon JI, Huttley GA, Kelley ST, Knights D, Koenig JE, Ley RE, Lozupone CA, McDonald D, Muegge BD, Pirrung M, Reeder J, Sevinsky JR, Turnbaugh PJ, Walters WA, Widmann J, Yatsunenko T, Zaneveld J, Knight R (2004) QIIME allows analysis of high-throughput community sequencing data. *Nat Methods* **7**, 335-336.

[67] Segata N, Izard J, Waldron L, Gevers D, Miropolsky L, Garrett WS, Huttenhower C (2011) Metagenomic biomarker discovery and explanation. *Genome Biol* **12**, R60.

[68] Langille MG, Zaneveld J, Caporaso JG, McDonald D, Knights D, Reyes JA, Clemente JC, Burkepile DE, Vega Thurber RL, Knight R, Beiko RG, Huttenhower C (2013) Predictive functional profiling of microbial communities using 16S rRNA marker gene sequences. *Nat Biotechnol* **31**, 814-821.

[69] Mosconi L, Pupi A, De Leon MJ (2008) Brain glucose hypometabolims and oxidative stress in preclinical Alzheimer's disease. *Ann N Y Acad Sci* **1147**, 180-195.

[70] Mosconi L, Berti V, Guyara-Quinn C, McHugh P, Petrongolo G, Osorio RS, Connaughty C, Pupi A, Vallabhajosula S, Isaacson RS, de Leon MJ, Swerdlow RH, Brinton RD (2017) Perimenopause and emergence of an Alzheimer's bioenergetic phenotype in brain and periphery. *PLoS One* **12**, e0185926.

[71] Végh MJ, Heldring CM, Kamphuis W, Hijazi S, Timmerman AJ, Li KW, van Nierop P, Mansvelder HD, Hol EM, Smit AB, van Kesteren RE (2014) Reducing hippocampal extracellular matrix reverses early memory deficits in a mouse model of Alzheimer's disease. *Acta Neuropathol Commun* **2**, 76.

[72] Bruce-Keller AJ, Gupta S, Knight AG, Beckett TL, McMullen JM, Davis PR, Murphy MP, Van Eldik LJ, St Clair D, Keller JN (2011) Cognitive impairment in humanized APP×PS1 mice is linked to Aβ(1-42) and NOX activation. *Neurobiol Dis* **44**, 317-326.

[73] Chen Y, Fang L, Chen S, Zhou H, Fan Y, Lin L, Li J, Xu J, Chen Y, Ma Y, Chen Y (2020) Gut microbiome alterations precede cerebral amyloidosis and microglial pathology in a mouse model of Alzheimer's disease. *Biomed Res Int* **2020**, 8456596.

[74] Bäuerl C, Collado MC, Diaz Cuevas A, Viña J, Pérez Martínez G (2018) Shifts in gut microbiota composition in an APP/PSS1 transgenic mouse model of Alzheimer's disease during lifespan. *Lett Appl Microbiol* **66**, 464-471.

[75] Harach T, Marungruang N, Duthilleul N, Cheatham V, Mc Coy KD, Frisoni G, Neher JJ, Fåk F, Jucker M, Lasser T, Bolmont T (2017) Reduction of Abeta amyloid pathology

in APPPS1 transgenic mice in the absence of gut micro-biota. *Sci Rep* **7**, 41802.

[76] Minter MR, Zhang C, Leone V, Ringus DL, Zhang X, Oyler-Castrillo P, Musch MW, Liao F, Ward JF, Holtzman DM, Chang EB, Tanzi RE, Sisodia SS (2016) Antibiotic-induced perturbations in gut microbial diversity influences neuro-inflammation and amyloidosis in a murine model of Alzheimer's disease. *Sci Rep* **6**, 30028.

[77] Zhang L, Wang Y, Xiayu X, Shi C, Chen W, Song N, Fu X, Zhou R, Xu Y, Huang L, Zhu H, Han Y, Qin C (2017) Altered gut microbiota in a mouse model of Alzheimer's disease. *J Alzheimers Dis* **60**, 1241-1257.

[78] Cox LM, Abou-El-Hassan H, Maghzi AH, Vincentini J, Weiner HL (2019) The sex-specific interaction of the microbiome in neurodegenerative diseases. *Brain Res* **1724**, 146385.

[79] Yao J, Irwin RW, Zhao L, Nilsen J, Hamilton RT, Brinton RD (2009) Mitochondrial bioenergetic deficit pre-cedes Alzheimer's pathology in female mouse model of Alzheimer's disease. *Proc Natl Acad Sci U S A* **106**, 14670-14675.

[80] Yao J, Hamilton RT, Cadenas E, Brinton RD (2010) Decline in mitochondrial bioenergetics and shift to keto-genic profile in brain during reproductive senescence. *Biochim Biophys Acta* **1800**, 1121-1126.

[81] Brinton RD, Yao J, Yin F, Mack WJ, Cadenas E (2015) Perimenopause as a neurological transition state. *Nat Rev Endocrinol* **11**, 393-405.

[82] Yin F, Yao J, Sancheti H, Feng T, Melcangi RC, Morgan TE, Finch CE, Pike CJ, Mack WJ, Cadenas E, Brinton RD (2015) The perimenopausal aging transition in the female rat brain: Decline in bioenergetic systems and synaptic plasticity. *Neurobiol Aging* **36**, 2282-2295.

[83] Ding F, Yao J, Rettberg JR, Chen S, Brinton RD (2013) Early decline in glucose transport and metabolism pre-cedes shift to ketogenic system in female aging and Alzheimer's mouse brain: Implication for bioenergetic intervention. *PLoS One* **8**, e79977.

[84] Krych Ł, Nielsen DS, Hansen AK, Hansen CH (2015) Gut microbial markers are associated with diabetes onset, regulatory imbalance, and IFN-γ level in NOD Mice. *Gut Microbes* **6**, 101-109.

[85] Chávez-Carbajal A, Pizano-Zárate ML, Hernández-Quiroz F, Ortiz-Luna GF, Morales-Hernández RM, De Sales-Millán A, Hernández-Trejo M, García-Vite A, Beltrán-Lagunes L, Hoyo-Vadillo C, García-Mena J (2020) Characterization of the gut microbiota of individu-als at different T2D stages reveals a complex relationship with the host. *Microorganisms* **8**, 94.

[86] Baothman OA, Zamzami MA, Taher I, Abubaker J, Abu-farha M (2016) The role of gut microbiota in the development of obesity and diabetes. *Lipids Health Dis* **15**, 108.

[87] Cox LM, Schafer MJ, Sohn J, Vincentini J, Weiner HL, Ginsberg SD, Blaser MJ (2019) Calorie restriction slows age-related microbiota changes in an Alzheimer's disease model in female mice. *Sci Rep* **9**, 17904.

[88] Berry D, Kuzyk O, Rauch I, Heider S, Schwab C, Hainzl E, Decker T, Müller M, Strobl B, Schleper C, Urich T, Wagner M, Kenner L, Loy A (2015) Intestinal micro-biota signatures associated with inflammation history in mice experiencing recurring colitis. *Front Microbiol* **6**, 1408.

[89] Teuber M (1985) The genus Lactococcus. In *The Gen-era of Lactic Acid Bacteria. The Lactic Acid Bacteria*,

Wood BJB, Holzapfel WH, eds. Springer, Boston, MA, pp. 173-234.

[90] Sheedy J, Wettenhall R, Scanlon D, Gooley P, Lewis D, McGregor N, Stapleton D, Butt H, DE Meirleier KL (2009) Increased D-Lactic acid intestinal bacteria in patients with chronic fatigue syndrome. *In Vivo* **23**, 621-628.

[91] Berchtold NC, Cribbs DH, Coleman PD, Rogers J, Head E, Kim R, Beach T, Miller C, Troncoso J, Trojanowski JQ, Zielke HR, Cotman CW (2008) Gene expression changes in the course of normal brain aging are sexually dimorphic. *Proc Natl Acad Sci U S A* **105**, 15605-15610.

[92] Mangold CA, Wronowski B, Du M, Masser DR, Hadad N, Bixler GV, Brucklacher RM, Ford MM, Sonntag WE, Freeman WM (2017) Sexually divergent induction of microglial-associated neuroinflammation with hippocam-pal aging. *J Neuroinflammation* **14**, 141.

[93] Flores R, Shi J, Fuhrman B, Xu X, Veenstra T, Gail M, Gajer P, Ravel J, Goedert JJ (2012) Fecal microbial determinants of fecal and systemic estrogens and estrogen metabolites: A cross-sectional study. *J Transl Med* **10**, 253.

[94] Huang R, Li T, Ni J, Bai X, Gao Y, Li Y, Zhang P, Gong Y (2018) Different sex-based responses of gut micro-biota during the development of hepatocellular carcinoma in liver-specific Tsc1-knockout mice. *Front Microbiol* **9**, 1008.

[95] Crost EH, Tailford LE, Le Gall G, Fons M, Henrissat B, Juge N (2013) Utilisation of mucin glycans by the human gut symbiont ruminococcus gnavus is strain-dependent. *PLoS One* **8**, e76341.

[96] Leclercq S, Matamoros S, Cani PD, Neyrinck AM, Jamar F, Stärkel P, Windey K, Tremaroli V, Bäckhed F, Verbeke K, de Timary P, Delzenne NM (2014) Intestinal perme-ability, gut-bacterial dysbiosis, and behavioral markers of alcohol-dependence severity. *Proc Natl Acad Sci U S A* **111**, E4485-E4493.

[97] Chen J, Chia N, Kalari KR, Yao JZ, Novotna M, Paz Sol-dan MM, Luckey DH, Marietta E V, Jeraldo PR, Chen X, Weinshenker BG, Rodriguez M, Kantarci OH, Nelson H, Murray JA, Mangalam AK (2016) Multiple sclerosis patients have a distinct gut microbiota compared to healthy controls. *Sci Rep* **6**, 28484.

[98] Javurek AB, Suresh D, Spollen WG, Hart ML, Hansen SA, Ellersieck MR, Bivens NJ, Givan SA, Upendran A, Kannan R, Rosenfeld CS (2017) Gut dysbiosis and neurobehavioral alterations in rats exposed to silver nanoparticles. *Sci Rep* **7**, 2822.

[99] Sun J, Ling Z, Wang F, Chen W, Li H, Jin J, Zhang H, Pang M, Yu J, Liu J (2016) Clostridium butyricum pretreatment attenuates cerebral ischemia/reperfusion injury in mice via anti-oxidation and anti-apoptosis. *Neurosci Lett* **613**, 30-35.

[100] Pisa D, Alonso R, Fernández-Fernández AM, Rábano A, Carrasco L (2017) Polymicrobial infections in brain tissue from Alzheimer's disease patients. *Sci Rep* **7**, 5559.

[101] Figueira J, Jonsson P, Nordin Adolfsson A, Adolfsson R, Nyberg L, Öhman A (2016) NMR analysis of the human saliva metabolome distinguishes dementia patients from matched controls. *Mol Biosyst* **12**, 2562-2571.

[102] Yilmaz A, Geddes T, Han B, Bahado-Singh RO, Wilson GD, Imam K, Maddens M, Graham SF (2017) Diagnostic biomarkers of Alzheimer's disease as identified in saliva using 1H NMR-based metabolomics. *J Alzheimers Dis* **58**, 355-359.

[103] LeBlanc JG, Chain F, Martín R, Bermúdez-Humarán LG, Courau S, Langella P (2017) Beneficial effects on host

energy metabolism of short-chain fatty acids and vitamins produced by commensal and probiotic bacteria. *Microb Cell Fact* **16**, 79.

[104] Ong L, Shah NP (2008) Influence of probiotic Lactobacillus acidophilus and L. helveticus on proteolysis, organic acid profiles, and ACE-inhibitory activity of cheddar cheeses ripened at 4, 8, and 12°C. *J Food Sci* **73**, M111-M120.

[105] Zhang C, Brandt MJ, Schwab C, Gänzle MG (2010) Propionic acid production by cofermentation of Lactobacillus buchneri and Lactobacillus diolivorans in sourdough. *Food Microbiol* **27**, 390-395.

[106] Xin Y, Diling C, Jian Y, Ting L, Guoyan H, Hualun L, Xiaocui T, Guoxiao L, Ou S, Chaoqun Z, Jun Z, Yizhen X (2018) Effects of oligosaccharides from morinda officinalis on gut microbiota and metabolome of APP/PS1 transgenic mice. *Front Neurol* **9**, 412.

[107] Bostanciklioğlu M (2019) The role of gut microbiota in pathogenesis of Alzheimer's disease. *J Appl Microbiol* **127**, 954-967.

[108] He Y, Li B, Sun D, Chen S (2020) Gut microbiota: Implications in Alzheimer's disease. *J Clin Med* **9**, 2042.

[109] Castro-González JM, Castro P, Sandoval H, Castro-Sandoval D (2019) Probiotic lactobacilli precautions. *Front Microbiol* **10**, 375.

[110] Sherid M, Samo S, Sulaiman S, Husein H, Sifuentes H, Sridhar S (2016) Liver abscess and bacteremia caused by lactobacillus: Role of probiotics? Case report and review of the literature. *BMC Gastroenterol* **16**, 138.

[111] Wallis A, Butt H, Ball M, Lewis DP, Bruck D (2016) Support for the microgenderome: Associations in a human clinical population. *Sci Rep* **6**, 19171.

[112] Gophna U, Konikoff T, Nielsen H (2017) Oscillospira and related bacteria - from metagenomic species to metabolic features. *Environ Microbiol* **19**, 835-841.

[113] Herrmann E, Young W, Rosendale D, Reichert-Grimm V, Riedel CU, Conrad R, Egert M (2017) RNA-based stable isotope probing suggests *Allobaculum* spp. as particularly active glucose assimilators in a complex murine microbiota cultured *in vitro*. *Biomed Res Int* **2017**, 1829685.

[114] Liu C, Li J, Zhang Y, Philip A, Shi E, Chi X, Meng J (2015) Influence of glucose fermentation on CO2 assimilation to acetate in homoacetogen Blautia coccoides GA-1. *J Ind Microbiol Biotechnol* **42**, 1217-1224.

[115] Vital M, Karch A, Pieper DH (2017) Colonic butyrate-producing communities in humans: An overview using omics data. *mSystems* **2**, e00130-17.

[116] Waters JL, Ley RE (2019) The human gut bacteria Christensenellaceae are widespread, heritable, and associated with health. *BMC Biol* **17**, 83.

[117] Zheng Y, Kahnt J, Kwon IH, Mackie RI, Thauer RK (2014) Hydrogen formation and its regulation in Ruminococcus albus: Involvement of an electron-bifurcating [FeFe]-hydrogenase, of a non-electron-bifurcating [FeFe]-hydrogenase, and of a putative hydrogen-sensing [FeFe]-hydrogenase. *J Bacteriol* **196**, 3840-3852.

[118] MacFabe DF (2015) Enteric short-chain fatty acids: Microbial messengers of metabolism, mitochondria, and mind: Implications in autism spectrum disorders. *Microb Ecol Health Dis* **26**, 28177.

[119] Shultz SR, Aziz NAB, Yang L, Sun M, MacFabe DF, O'Brien TJ (2015) Intracerebroventricular injection of propionic acid, an enteric metabolite implicated in autism, induces social abnormalities that do not differ between seizure-prone (FAST) and seizure-resistant (SLOW) rats. *Behav Brain Res* **278**, 542-548.

[120] MacFabe DF, Cain DP, Rodriguez-Capote K, Franklin AE, Hoffman JE, Boon F, Taylor AR, Kavaliers M, Ossenkopp KP (2007) Neurobiological effects of intraventricular propionic acid in rats: Possible role of short chain fatty acids on the pathogenesis and characteristics of autism spectrum disorders. *Behav Brain Res* **176**, 149-169.

[121] MacFabe DF, Cain NE, Boon F, Ossenkopp KP, Cain DP (2011) Effects of the enteric bacterial metabolic product propionic acid on object-directed behavior, social behavior, cognition, and neuroinflammation in adolescent rats: Relevance to autism spectrum disorder. *Behav Brain Res* **217**, 47-54.

[122] Govindarajan N, Agis-Balboa RC, Walter J, Sananbenesi F, Fischer A (2011) Sodium butyrate improves memory function in an alzheimer's disease mouse model when administered at an advanced stage of disease progression. *J Alzheimers Dis* **26**, 187-197.

[123] Huuskonen J, Suuronen T, Nuutinen T, Kyrylenko S, Salminen A (2004) Regulation of microglial inflammatory response by sodium butyrate and short-chain fatty acids. *Br J Pharmacol* **141**, 874-80.

[124] Kanski R, Sneeboer MA, van Bodegraven EJ, Sluijs JA, Kropff W, Vermunt MW, Creyghton MP, De Filippis L, Vescovi A, Aronica E, van Tijn P, van Strien ME, Hol EM (2014) Histone acetylation in astrocytes suppresses GFAP and stimulates a reorganization of the intermediate filament network. *J Cell Sci* **127**, 4368-4380.

[125] van der Velpen V, Teav T, Gallart-Ayala H, Mehl F, Konz I, Clark C, Oikonomidi A, Peyratout G, Henry H, Delorenzi M, Ivanisevic J, Popp J (2019) Systemic and central nervous system metabolic alterations in Alzheimer's disease. *Alzheimers Res Ther* **11**, 93.

[126] Gulaj E, Pawlak K, Bien B, Pawlak D (2010) Kynurenine and its metabolites in Alzheimer's disease patients. *Adv Med Sci* **55**, 204-211.